









TECH BRIEFS

NATIONAL AERONAUTICS AND SPACE ADMINISTRATION

-  **Technology Focus**
-  **Electronics/Computers**
-  **Software**
-  **Materials**
-  **Mechanics**
-  **Machinery/Automation**
-  **Manufacturing**
-  **Bio-Medical**
-  **Physical Sciences**
-  **Information Sciences**
-  **Books and Reports**

INTRODUCTION

Tech Briefs are short announcements of innovations originating from research and development activities of the National Aeronautics and Space Administration. They emphasize information considered likely to be transferable across industrial, regional, or disciplinary lines and are issued to encourage commercial application.

Availability of NASA Tech Briefs and TSPs

Requests for individual Tech Briefs or for Technical Support Packages (TSPs) announced herein should be addressed to

National Technology Transfer Center

Telephone No. (800) 678-6882 or via World Wide Web at www2.nttc.edu/leads/

Please reference the control numbers appearing at the end of each Tech Brief. Information on NASA's Commercial Technology Team, its documents, and services is also available at the same facility or on the World Wide Web at www.nctn.hq.nasa.gov.

Commercial Technology Offices and Patent Counsels are located at NASA field centers to provide technology-transfer access to industrial users. Inquiries can be made by contacting NASA field centers and program offices listed below.

NASA Field Centers and Program Offices

Ames Research Center

Carolina Blake
(650) 604-1754
carolina.m.blake@nasa.gov

Dryden Flight Research Center

Jenny Baer-Riedhart
(661) 276-3689
jenny.baer-riedhart@dfrc.nasa.gov

Goddard Space Flight Center

Nona Cheeks
(301) 286-5810
Nona.K.Cheeks.1@gsfc.nasa.gov

Jet Propulsion Laboratory

Art Murphy, Jr.
(818) 354-3480
arthur.j.murphy-jr@jpl.nasa.gov

Johnson Space Center

Charlene E. Gilbert
(281) 483-3809
commercialization@jsc.nasa.gov

Kennedy Space Center

Jim Aliberti
(321) 867-6224
Jim.Aliberti-1@ksc.nasa.gov

Langley Research Center

Jesse Midgett
(757) 864-3936
jesse.c.midgett@nasa.gov

John H. Glenn Research Center at Lewis Field

Larry Viterna
(216) 433-3484
cto@grc.nasa.gov

Marshall Space Flight Center

Vernotto McMillan
(256) 544-2615
vernotto.mcmillan@msfc.nasa.gov

Stennis Space Center

Robert Bruce
(228) 688-1929
robert.c.bruce@nasa.gov

NASA Program Offices

At NASA Headquarters there are seven major program offices that develop and oversee technology projects of potential interest to industry:

Carl Ray

Small Business Innovation Research Program (SBIR) & Small Business Technology Transfer Program (STTR)
(202) 358-4652 or
cray@mail.hq.nasa.gov

Benjamin Neumann

Innovative Technology Transfer Partnerships (Code RP)
(202) 358-2320
benjamin.j.neumann@nasa.gov

John Mankins

Office of Space Flight (Code MP)
(202) 358-4659 or
jmankins@mail.hq.nasa.gov

Terry Hertz

Office of Aero-Space Technology (Code RS)
(202) 358-4636 or
thertz@mail.hq.nasa.gov

Glen Mucklow

Office of Space Sciences (Code SM)
(202) 358-2235 or
gmucklow@mail.hq.nasa.gov

Roger Crouch

Office of Microgravity Science Applications (Code U)
(202) 358-0689 or
rcrouch@hq.nasa.gov

Granville Paules

Office of Mission to Planet Earth (Code Y)
(202) 358-0706 or
gpaules@mtpe.hq.nasa.gov



TECH BRIEFS

NATIONAL AERONAUTICS AND SPACE ADMINISTRATION



5 Technology Focus: Test & Measurement

- 5 Simulation Testing of Embedded Flight Software
- 5 Improved Indentation Test for Measuring Nonlinear Elasticity
- 6 Ultraviolet-Absorption Spectroscopic Biofilm Monitor
- 7 Electronic Tongue for Quantitation of Contaminants in Water
- 7 Radar for Measuring Soil Moisture Under Vegetation



9 Electronics/Computers

- 9 Modular Wireless Data-Acquisition and Control System
- 9 Microwave System for Detecting Ice on Aircraft
- 10 Routing Algorithm Exploits Spatial Relations
- 11 Two-Finger EKG Method of Detecting Evasive Responses



13 Software

- 13 Updated System-Availability and Resource-Allocation Program
- 13 Routines for Computing Pressure Drops in Venturis
- 13 Software for Fault-Tolerant Matrix Multiplication



15 Materials

- 15 Reproducible Growth of High-Quality Cubic-SiC Layers
- 16 Nonlinear Thermoelastic Model for SMAs and SMA Hybrid Composites
- 17 Liquid-Crystal Thermosets, a New Generation of High-Performance Liquid-Crystal Polymers
- 18 Formulations for Stronger Solid Oxide Fuel-Cell Electrolytes



19 Mechanics

- 19 Simulation of Hazards and Poses for a Rocker-Bogie Rover

- 20 Autonomous Formation Flight
- 21 Expandable Purge Chambers Would Protect Cryogenic Fittings
- 22 Wavy-Planform Helicopter Blades Make Less Noise



23 Machinery/Automation

- 23 Miniature Robotic Spacecraft for Inspecting Other Spacecraft
- 23 Miniature Ring-Shaped Peristaltic Pump
- 24 Compact Plasma Accelerator
- 25 Improved Electrohydraulic Linear Actuators
- 26 A Software Architecture for Semiautonomous Robot Control



27 Manufacturing

- 27 Fabrication of Channels for Nanobiotechnological Devices
- 27 Improved Thin, Flexible Heat Pipes



29 Physical Sciences

- 29 Miniature Radioisotope Thermoelectric Power Cubes
- 29 Permanent Sequestration of Emitted Gases in the Form of Clathrate Hydrates
- 30 Electrochemical, H₂O₂-Boosted Catalytic Oxidation System
- 30 Electrokinetic In Situ Treatment of Metal-Contaminated Soil
- 31 Pumping Liquid Oxygen by Use of Pulsed Magnetic Fields
- 32 Magnetocaloric Pumping of Liquid Oxygen



33 Books & Reports

- 33 Tailoring Ion-Thruster Grid Apertures for Greater Efficiency
- 33 Lidar for Guidance of a Spacecraft or Exploratory Robot

This document was prepared under the sponsorship of the National Aeronautics and Space Administration. Neither the United States Government nor any person acting on behalf of the United States Government assumes any liability resulting from the use of the information contained in this document, or warrants that such use will be free from privately owned rights.



Simulation Testing of Embedded Flight Software

NASA's Jet Propulsion Laboratory, Pasadena, California

Virtual Real Time (VRT) is a computer program for testing embedded flight software by computational simulation in a workstation, in contradistinction to testing it in its target central processing unit (CPU). The disadvantages of testing in the target CPU include the need for an expensive test bed, the necessity for testers and programmers to take turns using the test bed, and the lack of software tools for debugging in a real-time environment. By virtue of its architecture, most of the flight software of the type in question is amenable to development and testing on workstations, for which there is an abundance of commercially available debugging and analysis software tools.

Unfortunately, the timing of a workstation differs from that of a target CPU in a test bed. VRT, in conjunction with closed-loop simulation software, provides a capability for executing embedded flight software on a workstation in a close-to-real-time environment. A scale factor is used to convert between execution time in VRT on a workstation and execution on a target CPU. VRT includes high-resolution operating-system timers that enable the synchronization of flight software with simulation software and ground software, all running on different workstations.

This program was written by Mohammad Shahabuddin and William Reinholtz of Caltech for NASA's Jet Propulsion Laboratory.

Further information is contained in a TSP (see page 1).

In accordance with Public Law 96-517, the contractor has elected to retain title to this invention. Inquiries concerning rights for its commercial use should be addressed to:

*Innovative Technology Assets Management
JPL*

*Mail Stop 202-233
4800 Oak Grove Drive
Pasadena, CA 91109-8099
(818) 354-2240*

*E-mail: iaoffice@jpl.nasa.gov
Refer to NPO-30689, volume and number of this NASA Tech Briefs issue, and the page number.*

Improved Indentation Test for Measuring Nonlinear Elasticity

This technique is especially useful for characterizing thermal-barrier coating materials.

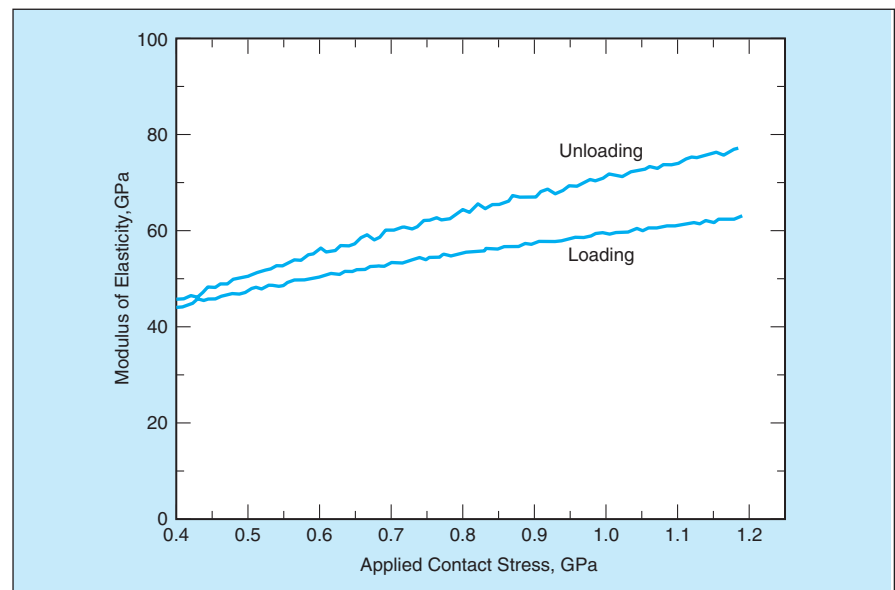
John H. Glenn Research Center, Cleveland, Ohio

A cylindrical-punch indentation technique has been developed as a means of measuring the nonlinear elastic responses of materials — more specifically, for measuring the moduli of elasticity of materials in cases in which these moduli vary with applied loads. This technique offers no advantage for characterizing materials that exhibit purely linear elastic responses (constant moduli of elasticity, independent of applied loads). However, the technique offers a significant advantage for characterizing such important materials as plasma-sprayed thermal-barrier coatings, which, in cyclic loading, exhibit nonlinear elasticity with hysteresis related to compaction and sliding within their microstructures.

A specimen to be tested by the cylindrical-punch indentation technique is prepared by standard metallographic procedures. The specimen is mounted on a load-versus-displacement-measuring apparatus, which could be any of a variety of indentation-type hardness testers or other conventional mechanical testing instruments. In the indentation test, the flat end of a round cylin-

dricul punch is pushed into the polished, flat surface of the specimen. To minimize impression creep (a time-dependent plastic deformation that could

contribute a large error to the modulus data), the specimen is preconditioned by pre-indenting it at a load greater than the load to be applied during the subse-



These Plots of Modulus of Elasticity as a function of applied stress were calculated from displacement-vs.-load data for a 127- μm -diameter flat-bottom cylindrical tungsten carbide punch against a thermal-barrier coating of plasma-sprayed ZrO_2 containing 8 weight percent of Y_2O_3 during the third loading/unloading cycle of an indentation.

quent test. Thereafter, the applied load is varied according to the specification for the test and the punch displacement is measured as a function of the applied load. The modulus of elasticity (for example, see figure) and, if desired, other aspects of the elastic response of the specimen material are computed from the displacement-versus-load data with corrections, if necessary, for the elastic response of the punch and the rest of the testing apparatus.

The flat-bottom cylindrical punch used in this technique offers important advantages over the pointed indenters used in traditional hardness testing: A pointed indenter is well suited to measuring hardness but is ill suited to measuring the

modulus of elasticity of a specimen because the contact area is unknown and varies during the test, so that there is no simple relationship between applied load and applied stress. In addition, a pointed indenter causes significant plastic deformation (even at nearly zero applied load), which cannot easily be distinguished from elastic deformation. In contrast, while the flat-bottom cylindrical punch is useless for hardness testing, it is well suited for measuring the modulus of elasticity because its contact area is constant and, consequently, the applied stress is simply proportional to the applied load. Hence, the modulus of elasticity can be determined at every point on the load-versus-displacement curve. Also,

if the applied load is limited to below the value corresponding to the contact stress at the onset of plastic deformation, the deformation can be relied upon to be elastic over a complete loading/unloading cycle, making it unnecessary to subtract the effects of plastic deformation.

This work was done by Jeffrey I. Eldridge of Glenn Research Center. Further information is contained in a TSP (see page 1).

Inquiries concerning rights for the commercial use of this invention should be addressed to NASA Glenn Research Center, Commercial Technology Office, Attn: Steve Fedor, Mail Stop 4-8, 21000 Brookpark Road, Cleveland Ohio 44135. Refer to LEW-17412.

Ultraviolet-Absorption Spectroscopic Biofilm Monitor

Continuous monitoring could provide early warnings of potentially harmful buildups of bacteria.

Lyndon B. Johnson Space Center, Houston, Texas

An ultraviolet-absorption spectrometer system has been developed as a prototype instrument to be used in continuous, real-time monitoring to detect the growth of biofilms. Such monitoring is desirable because biofilms are often harmful. For example, biofilms in potable-water and hydroponic systems act as both sources of pathogenic bacteria that resist biocides and as a mechanism for deterioration (including corrosion) of pipes.

Biofilms formed from several types of hazardous bacteria can thrive in both plant-growth solutions and low-nutrient media like distilled water. Biofilms can also form in condensate tanks in air-condition-

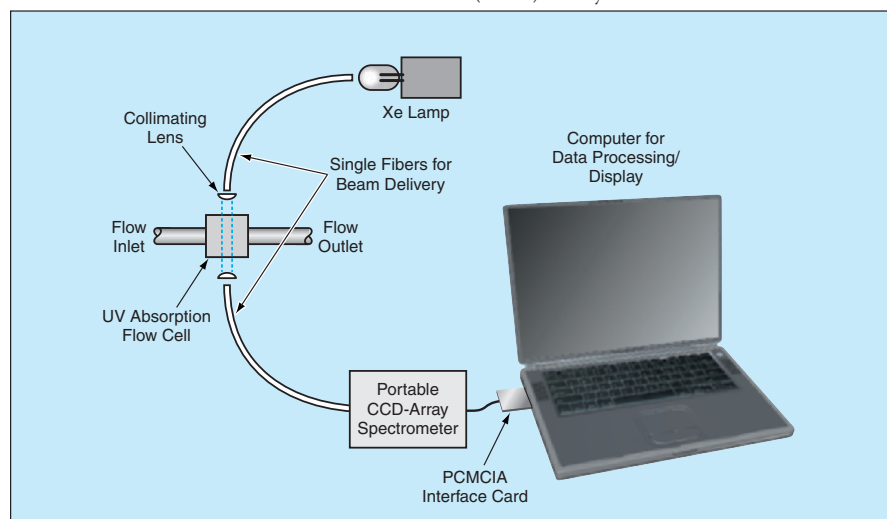
ing systems and in industrial heat exchangers. At present, bacteria in potable-water and plant-growth systems aboard the space shuttle (and previously on the *Mir* space station) are monitored by culture-plate counting, which entails an incubation period of 24 to 48 hours for each sample. At present, there are no commercially available instruments for continuous monitoring of biofilms in terrestrial or spaceborne settings.

The prototype biofilm monitor includes a commercial fiber-optic-coupled ultraviolet/visible (UV/VIS) spectrometer module with charge-coupled-device (CCD) array detection that has dimen-

sions of 6 by 6 by 2 in. (about 15 by 15 by 5 cm) and that communicates with a notebook computer via a Personal Computer Memory Card International Association (PCMCIA) interface card. The instrument includes two 4-ft (1.2-m)-long optical fibers — one for coupling light from a xenon source to a flow-cell/fiber sensor assembly, the other for coupling light from the flow-cell/fiber sensor assembly to the spectrometer module. In the flow-cell/fiber sensor assembly, the ends of the fibers are coupled into the quartz windows of the cell with small collimating lenses. The inner surfaces of the windows are in contact with the flowing water to be monitored.

In tests of the prototype biofilm monitor, biofilms were found to produce characteristic absorption spectral bands at wavelengths from 230 to 400 nm. The absorption bands obtained from biofilms grown from a single strain of *Pseudomonas aeruginosa* were found to differ from the absorption bands obtained from biofilms grown from a mixed bacterial population from untreated urban river water; thus, it appears possible to use instruments of this type not only to detect biofilms but also to distinguish among species of bacteria in biofilms.

This work was done by Ronald H. Micheels of Polestar Technologies, Inc., for Johnson Space Center. Further information is contained in a TSP (see page 1).
MSC-22882



The **UV Absorption Spectroscopic Biofilm Monitor System** is based on a miniature UV/VIS spectrometer with a fiber-optic input and a CCD-array detector. This instrument measures UV absorption spectra of biofilms that form on the inner surfaces of quartz windows of a flow cell.

Electronic Tongue for Quantitation of Contaminants in Water

The main advantage is ruggedness.

NASA's Jet Propulsion Laboratory, Pasadena, California

An assembly of sensors, denoted an electronic tongue, is undergoing development as a prototype of compact devices for use in measuring concentrations of contaminants in water. Thus far, the electronic tongue has been tested on ions of Cu, Zn, Pb, and Fe and shown to respond to concentrations as low as about 10 parts per million. This electronic tongue is expected to be ca-

pable of measuring concentrations of other metal ions and organic compounds. Potential uses for electronic tongues include monitoring the chemical quality of water in a variety of natural, industrial, and laboratory settings; detecting micro-organisms indirectly by measuring microbially influenced corrosion; and characterizing compounds of interest to the pharmaceutical and

food industries.

This version of the electronic tongue includes a heater, a temperature sensor, an array of ion-specific electrodes, an oxidation/reduction sensor pair, an electrical-conductivity sensor, and an array of galvanic cells, all on one compact ceramic substrate (see figure). Special-purpose electronic excitation and readout circuitry for the sensors has also been constructed.

The main advantage of the electronic tongue, relative to electrodes of this type used traditionally to assess water quality, is extreme ruggedness.

The types of measurements that can be performed by use of the sensors on the electronic tongue are quite varied. The best combination of types of measurements for a given application depends on the specific contaminants that one seeks to detect. Experimental studies to identify such combinations were in progress at the time of reporting the information for this article.

This work was done by Marlin Buehler and Gregory Kuhlman of Caltech for NASA's Jet Propulsion Laboratory. Further information is contained in a TSP (see page 1).

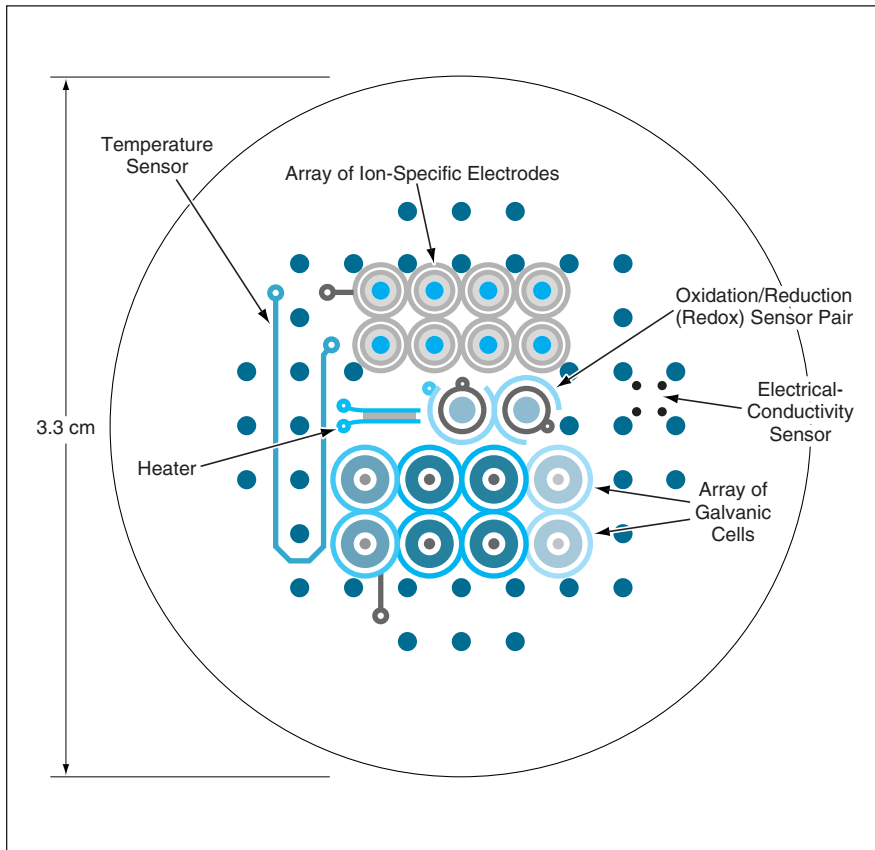
In accordance with Public Law 96-517, the contractor has elected to retain title to this invention. Inquiries concerning rights for its commercial use should be addressed to:

*Innovative Technology Assets Management
JPL*

*Mail Stop 202-233
4800 Oak Grove Drive
Pasadena, CA 91109-8099
(818) 354-2240*

E-mail: iaoffice@jpl.nasa.gov

Refer to NPO-30601, volume and number of this NASA Tech Briefs issue, and the page number.



A Heater and Sensors of Five Different Types are all mounted together on a compact ceramic substrate.

Radar for Measuring Soil Moisture Under Vegetation

Polarimetric data would be acquired at two frequencies.

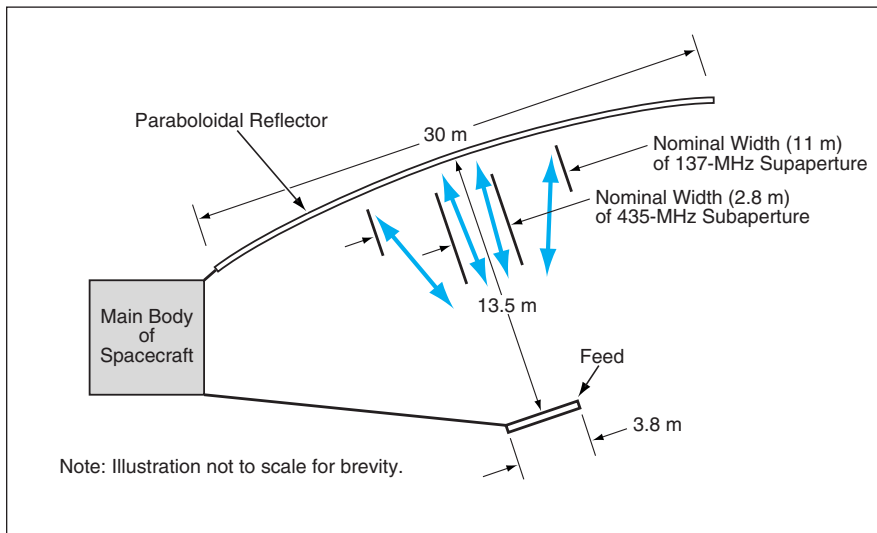
NASA's Jet Propulsion Laboratory, Pasadena, California

A two-frequency, polarimetric, spaceborne synthetic-aperture radar (SAR) system has been proposed for measuring the moisture content of soil as a function of depth, even in the presence of overlying vegetation. These measurements are needed because data on soil moisture

under vegetation canopies are not available now and are necessary for completing mathematical models of global energy and water balance with major implications for global variations in weather and climate.

The two proposed frequencies (137 and 435 MHz) are low relative to frequencies

ordinarily used in radar systems. One reason for choosing these frequencies is that they are low enough to enable penetration of vegetation and of soil to the required depths. Another reason for choosing these frequencies, in conjunction with polarimetry, is that prior research has shown



A **Lightweight Paraboloidal Mesh Reflector** would be subilluminated by a feed that would generate fan-shaped beams at 137 and 435 MHz.

that measurement data from at least two frequencies and multiple polarizations are needed to make it possible to separate the vegetation-canopy and soil contributions to the radar returns so as to be able to estimate the soil moisture content.

One of the principal challenges in designing the proposed system is posed by the need for a large antenna to form the required polarimetric measurement swath at the two chosen frequencies. A current state-of-the-art design would entail an antenna-and-feed mass of about 3 tons (≈ 2.7 tonnes), which would be im-

practically heavy. In contrast, the antenna and its feed in the proposed system would weigh only about one-tenth as much. In addition, the antenna could be stowed compactly during launch into orbit.

The proposed antenna (see figure) would include a lightweight paraboloidal mesh reflector about 30 m wide. A dual-polarization stack-patch array feed would generate beams having a highly controlled fan-like shape to subilluminate the reflector in synthesized approximately rectangular apertures: the feed would be designed and operated so that its radiation pattern

would synthesize a 30-by-11-m aperture at 137 MHz and a 30-by-2.8-m aperture at 435 MHz. The feed would have dimensions of about 3.8 by 1.2 by 0.1 m.

Another principal challenge in designing the proposed system is to refine and verify the algorithms used to retrieve soil moisture contents at depths ranging from centimeters to meters under substantial vegetation. Such retrievals involve inversion of mathematical models that (1) characterize vegetation and its interaction with soil and (2) represent soil as a multilayered medium containing random boundaries and varying permittivity. The details of such retrievals are complex and require detailed sensitivity analyses and demonstrations with real measurement data. Planned development efforts include experiments using a simple tower-based radar system to obtain data to estimate soil moisture contents and compare the estimates with actual values obtained by use of soil-moisture probes. It will also be necessary to optimize the design to minimize the adverse effects of propagation of radar signals through the ionosphere and to develop post-processing algorithms to correct for what remains of these effects after optimization of design.

This work was done by Mahta Moghadam, Delwyn Moller, Ernesto Rodriguez, and Yahya-Rahmat-Samii of Caltech for NASA's Jet Propulsion Laboratory. Further information is contained in a TSP (see page 1). NPO-30666



Modular Wireless Data-Acquisition and Control System

This system can be used to build an autonomous, highly reliable instrumentation network.

John F. Kennedy Space Center, Florida

A modular wireless data-acquisition and control system, now in operation at Kennedy Space Center, offers high performance at relatively low cost. The system includes a central station and a finite number of remote stations that communicate with each other through low-power radio-frequency (RF) links. Designed to satisfy stringent requirements for reliability, integrity of data, and low power consumption, this system could be reproduced and adapted to use in a broad range of settings. Examples of potential applications include industrial instrumentation, home automation, wireless intrusion-detection systems, remote reading of meters, medical instrumentation, telecommunications, automotive systems, homeland security, and military reconnaissance.

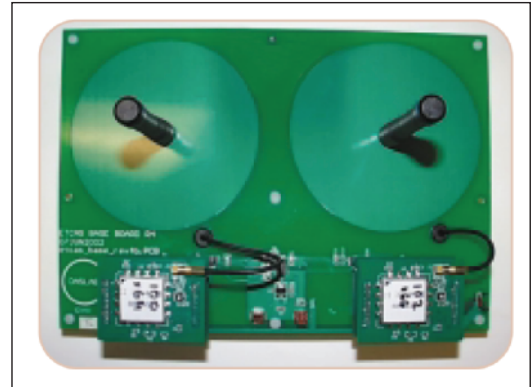
The central station has been implemented on several platforms, such as single board computers, personal computers, and the like, running custom software developed by NASA. Through its RS-232 port (a standard port for asynchronous serial data communication), the central station is connected to radio-transceiver modules (see figure) identical to the corresponding modules in the remote stations.

The remote stations contain programmable microcontrollers that can be easily reconfigured to perform many functions, depending on the application. For example, the microcontrollers can buffer data, process data, provide excitation for sensors, perform signal-conditioning and conversion functions, and control local equipment. The microcontroller architecture can easily accommodate local

“smart sensor” instrumentation that has self-calibration and self-diagnosis capabilities. Moreover, by suitable processing of data, the microcontrollers gain the ability to make decisions regarding operation and regarding the selection of relevant information to send to the central station; as a result, the bandwidth needed for communication is reduced and the system can be made less complex than it would otherwise be.

The remote stations include power-management modules. An efficient power-management scheme enables the remote stations to operate on batteries for several years (sampling rate dependent). Each remote station stays in a low-power-consumption mode until either it receives a message from the central station or another event triggers its power-management module to supply power to the other modules.

The output power of the radio transmitter in each station is made low (≈ 10 mW) to minimize interference. The range of each station is 300 feet (about 90 m) with a small whip antenna and can be increased by use of a directional antenna. The system is based on a spread-spectrum transceiver and uses an in-house developed algorithm to central communication over more than 100 frequency pairs on a 433- or 918-MHz base frequency. The wireless links currently operate at a data rate of 19.2 kb/s, but are capable of 115 kb/s.



The **Central Station Hardware** includes communication modules that contain generic RF circuit boards. Identical communication modules are used in the remote stations.

The central station normally communicates with all remote stations directly, but the system can reconfigure itself to restore communication when a remote station moves out of range or interference occurs. Upon loss of the RF signal from a remote station, the central station initiates a routine to determine which remote station(s) can become a relay for the lost station. The routine can occur on multiple levels to create a chain of stations and thereby enable long-distance communication using relatively low power.

This work was done by José Perotti and Angel Lucena of Kennedy Space Center and Pedro Medelius, Carlos Mata, Anthony Eckhoff, and Norman Blalock of ASRC Aerospace. For further information, contact the Kennedy Commercial Technology Office at (321) 867-8130. KSC-12386

Microwave System for Detecting Ice on Aircraft

This system can distinguish among ice, water, and ice/water mixtures.

John H. Glenn Research Center, Cleveland, Ohio

A microwave-based system has been developed as a means of detecting ice on aircraft surfaces, with enough sensitivity to provide a warning before the ice accretes to a dangerous thickness.

The system can measure the thickness of ice from a few mils (1 mil = 0.0254 mm) to about 1/4 in. (≈ 6 mm) and can distinguish among (1) ice, (2) water (or deicing fluid), and (3) a mixture of

ice and water (or deicing fluid). Sensors have been ruggedized to withstand the rain erosion environment.

The system (see Figure 1) includes a microwave module that contains a con-

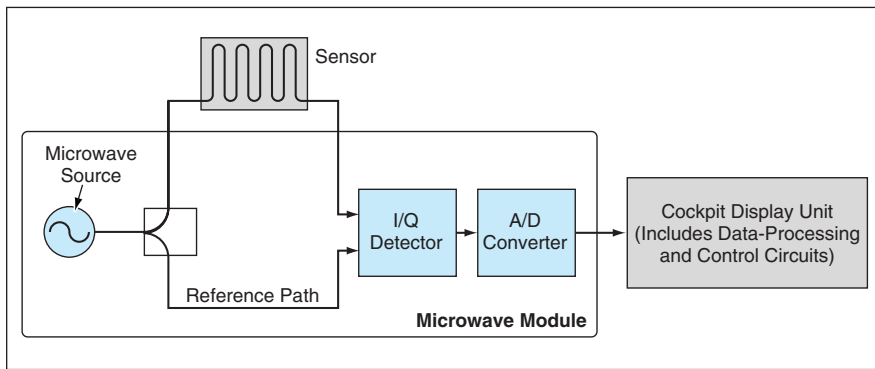


Figure 1. The Sensor Is a Section of CPW or SL Transmission Line flush with an aircraft surface. The magnitude and phase of the microwave signal arriving at the I/Q detector is affected by the amount of ice and/or water coating the sensory section of the transmission line.

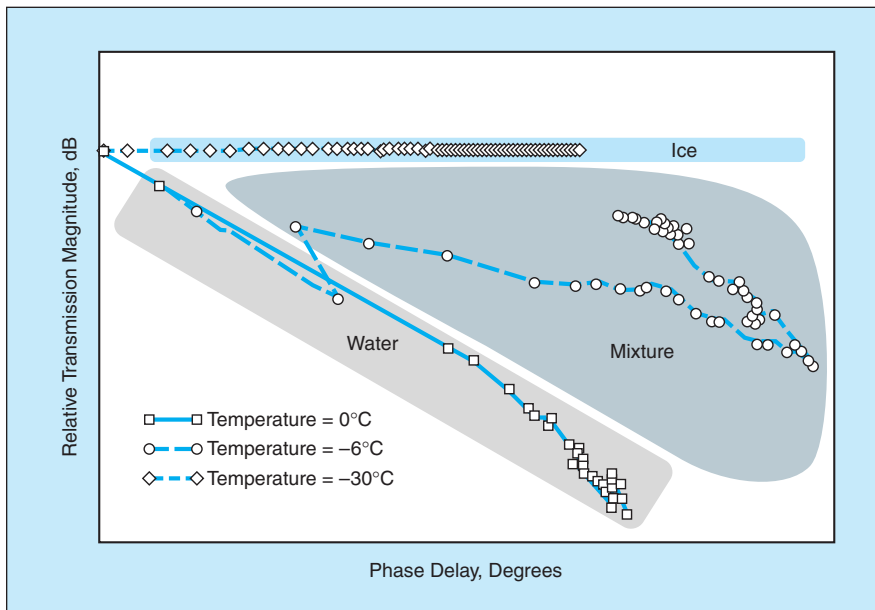


Figure 2. This Normalized Response in the Magnitude/Phase Plane was obtained in tests of a slot-line sensor at three temperatures. Three distinct regions of the magnitude-vs.-phase plane make it possible to distinguish among coats of ice, water, and mixtures thereof. In the important case of pure ice, the amplitude shift is negligible and the thickness of ice is indicated by the amount of phase shift.

tinuous-wave microwave signal source, the output of which is split onto a sensor path and a reference path. The sensor path consists of a microwave transmission line that includes a sensory portion of either the ground-plane coplanar-waveguide (CPW) type or the slot-line (SL) type. Whichever type is used, the sensory portion of the transmission line is mounted flush with the aircraft surface at the desired ice-detection location. With the exception of the sensory portion of the transmission line, the aforementioned circuitry is enclosed within an electrically conductive box. The sensor- and reference-path outputs are processed through an in-phase/quadrature (I/Q) detector, then through an analog-to-digital (A/D) converter. The output of the A/D converter is sent to data-processing and control circuitry in a cockpit display unit.

The data-processing subsystem computes the magnitude and phase of the sensor signal relative to those of the reference signal, and uses the sensor signal obtained when the sensor is bare to normalize the response of the system when water and/or ice are present. The normalized magnitude and phase response of the system serves as an indication of the thickness of ice and or water (see Figure 2).

This work was done by Philip J. Joseph, Dennis P. Glynn III, and John C. Joseph of Dedicated Electronics, Inc., for Glenn Research Center.

Inquiries concerning rights for the commercial use of this invention should be addressed to NASA Glenn Research Center, Commercial Technology Office, Attn: Steve Fedor, Mail Stop 4-8, 21000 Brookpark Road, Cleveland, Ohio 44135. Refer to LEW-17135.

Routing Algorithm Exploits Spatial Relations

This algorithm is competitive with two prior algorithms.

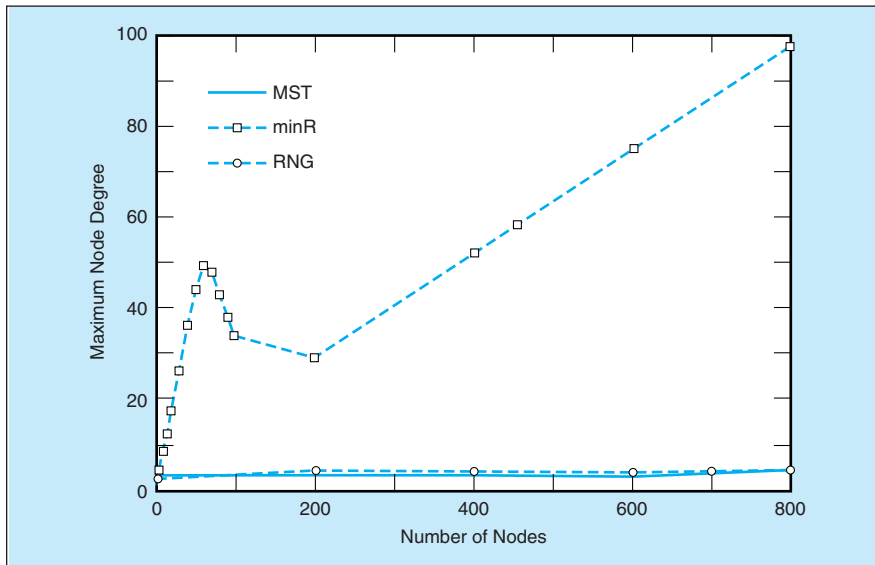
NASA's Jet Propulsion Laboratory, Pasadena, California

A recently developed routing algorithm for broadcasting in an *ad hoc* wireless communication network takes account of, and exploits, the spatial relationships among the locations of nodes, in addition to transmission power levels and distances between the nodes. In contrast, most prior algorithms for discovering routes through *ad hoc* networks rely heavily on transmission power levels and utilize limited graph-topology techniques that do not involve consideration of the aforesaid spatial relationships. The present algorithm extracts

the relevant spatial-relationship information by use of a construct denoted the relative-neighborhood graph (RNG).

The RNG algorithm is best described by reference to, and comparison with, two prior algorithms: one based on a construct denoted the minimum-radius (minR) graph, the other based on a construct denoted the minimum spanning tree (MST). The minR algorithm starts from the assumption that every node must use the same transmission radius, d . [As used here, "transmission radius" does

not signify radius as the term is commonly understood; instead, it signifies an effective radius that depends on the ratio between the transmission power and the bit rate.] An iterative binary search is performed to find the smallest d that guarantees connectivity of the network. On each iteration, a graph with transmission radius d is computed. If the graph is found to be connected, then d is decreased for the next iteration. The algorithm stops at the finding of the value of d such that the graph is connected but at the next smaller



The **Maximum Node Degree** as a function of the number of nodes was computed for each of the three algorithms by averaging results from 1,000 computational simulations. (The degree of a given node is defined as the number of neighboring nodes that communicate directly with the given node. A higher node degree implies the need to schedule more time for communication via the given node.)

increment of d , the graph is partitioned into two or more sub-graphs. The number of operations needed to compute the minR graph is proportional to a number of the order of $n^2 \log(s)$, where n is the number of nodes and s is the length of the side of a square of the same area as that containing the nodes.

The RNG of a set of nodes is the graph constructed according to the rule that any two of the nodes separated by distance l are connected by an edge only if there does not exist another node at a distance $< l$ from either first-mentioned node. The two nodes so connected are denoted relative

neighbors. In the RNG, unlike in the minR graph, a different radius can be used for each pair of nodes. The RNG is a super-graph of the MST (which is described next) and a sub-graph of the graph of the Delaunay triangulation, which is a technique for connecting pairs of grid points with straight lines in such a way as to obtain an optimum tessellation of a grid area. The number of operations needed to compute the RNG is proportional to a number of the order of $n \log(n)$.

The MST is a sub-graph of the RNG. Therefore, one can use the RNG in the computation of the MST. An edge is in-

cluded in the MST if it does not create a cycle in the graph. The construction of the MST involves disjoint sets. Nodes that are connected are placed in the same set. If a tested edge connects two nodes belonging to different sets, then the edge is added to MST and the two sets are united. If a tested edge connects two nodes belonging to the same set, then this edge creates a cycle and it is rejected. The number of operations needed to compute the MST is bounded by a number proportional to n , given that the RNG was pre-computed.

The comparison among the three algorithms is unavoidably complex because each offers both advantages and disadvantages with respect to the others. The figure presents an example of comparison with respect to the maximum node degree, which is only one of several different measures applied to results of computational simulations. The only general conclusion that one can draw from the comparisons by this and other measures is that the graph properties of the RNG are good, relative to those of the minR graph and the MST and that the RNG is suitable for efficient dissemination of information to all the nodes of a network.

This work was done by Clayton Okino and Esther Jennings of Caltech for NASA's Jet Propulsion Laboratory. Further information is contained in a TSP (see page 1).

This algorithm is available for commercial licensing. Please contact Don Hart of the California Institute of Technology at (818) 393-3425. Refer to NPO-30453.

Two-Finger EKG Method of Detecting Evasive Responses

John H. Glenn Research Center, Cleveland, Ohio

A system based on acquisition and processing of electrocardiographic (EKG) signals from two fingers has been proposed as a means of determining whether a person is answering questions evasively. The system — in effect, a “lie detector” of sorts, would be used to gauge prospective passengers’ responses to questions at airport security checkpoints. The person to be interrogated would be required to put one finger from each hand onto two metal strips on a counter and would be in-

structed to relax and wait for the system to indicate that it is ready. Then a security person would ask the passenger a set of standard security questions. EKG signals acquired through contact with the fingers would be processed by an algorithm that would extract a single-value measure of the level of stress in the interrogated person. This measure would be used to determine whether the system should display a green or a red light to signify that the person is or is not, respectively, telling

the truth. It has also been conjectured that the system may be useful for communicating with a person who is in a coma and, hence, unable to speak.

This work was done by Daniel Oldham of Glenn Research Center.

Inquiries concerning rights for the commercial use of this invention should be addressed to NASA Glenn Research Center, Commercial Technology Office, Attn: Steve Fedor, Mail Stop 4-8, 21000 Brookpark Road, Cleveland Ohio 44135. Refer to LEW-17441-1.

2 Updated System-Availability and Resource-Allocation Program

A second version of the Availability, Cost and Resource Allocation (ACARA) computer program has become available. The first version was reported in "System-Availability and Resource-Allocation Program" (LEW-15713), *NASA Tech Briefs*, Vol. 19, No. 8 (August 1995), page 54. To recapitulate: ACARA analyzes the availability, mean-time-between-failures of components, life-cycle costs, and scheduling of resources of a complex system of equipment. ACARA uses a statistical Monte Carlo method to simulate the failure and repair of components while complying with user-specified constraints on spare parts and resources. ACARA evaluates the performance of the system on the basis of a mathematical model developed from a block-diagram representation. The previous version utilized the MS-DOS operating system and could not be run by use of the most recent versions of the Windows operating system. The current version incorporates the algorithms of the previous version but is compatible with Windows and utilizes menus and a file-management approach typical of Windows-based software.

This program was written by Larry Viterna and Dale Stalnakar of Glenn Research Center. Further information is contained in a TSP (see page 1).

Inquiries concerning rights for the commercial use of this invention should be addressed to NASA Glenn Research Center, Commercial Technology Office, Attn: Steve Fedor, Mail Stop 4-8, 21000 Brookpark Road, Cleveland, Ohio 44135. Refer to LEW-17308.

4 Routines for Computing Pressure Drops in Venturis

A set of computer-program routines has been developed for calculating pressure drops and recoveries of flows through standard venturis, nozzle venturis, and orifices. Relative to prior methods used for such calculations, the method implemented by these routines offers greater accuracy because it involves fewer simplifying assumptions and is more generally applicable to wide ranges of flow conditions. These routines are based on conservation of momentum and energy equations for real nonideal fluids, the properties of which are calculated by curve-fitting subroutines based on empirical properties data. These routines are capable of representing cavitating, choked, non-cavitating, and unchoked flow conditions for liquids, gases, and supercritical fluids. For a computation of flow through a given venturi, nozzle venturi, or orifice, the routines determine which flow condition occurs: First, they calculate a throat pressure under the assumption that the flow is unchoked or non-cavitating, then they calculate the throat pressure under the assumption that the flow is choked or cavitating. The assumption that yields the higher throat pressure is selected as the correct one.

This program was written by Laurence de Quay of Stennis Space Center.

Inquiries concerning rights for the commercial use of this invention should be addressed to the Intellectual Property Manager, Stennis Space Center, (228) 688-1929. Refer to SSC-00161.

6 Software for Fault-Tolerant Matrix Multiplication

Formal Linear Algebra Recovery Environment is a computer program for high-performance, fault-tolerant matrix multiplication. The program is based on an extension of the prior theory and practice of fault-tolerant matrix-matrix multiplication of the form $C = AB$. This extension provides low-overhead methods for detecting errors, not only in C , but also in A and/or B . These methods enable the detection of all errors as long as, in a given case, only one entry in A , B , or C is corrupted. The program also provides for following a low-overhead rollback approach to correct errors once detected. Results of computational experiments have demonstrated that the methods implemented in this program work well in practice while imposing an acceptably low level of overhead, relative to high-performance matrix-multiplication methods that do not afford fault tolerance.

This program was written by Daniel Katz, Edwin Tisdale, Enrique Quintana-Ortí, John Gunnels, and Robert van de Geijn of Caltech for NASA's Jet Propulsion Laboratory. Further information is contained in a TSP (see page 1).

This software is available for commercial licensing. Please contact Don Hart of the California Institute of Technology at (818) 393-3425. Refer to NPO-30395.



Reproducible Growth of High-Quality Cubic-SiC Layers

Cubic SiC could be used to improve high-power and harsh-environment electronic devices.

John H. Glenn Research Center, Cleveland, Ohio

Semiconductor electronic devices and circuits based on silicon carbide (SiC) are being developed for use in high-temperature, high-power, and/or high-radiation conditions under which devices made from conventional semiconductors cannot adequately perform. The ability of SiC-based devices to function under such extreme conditions is expected to enable significant improvements in a variety of applications and systems. These include greatly improved high-voltage switching for saving energy in public electric power distribution and electric motor drives; more powerful microwave electronic circuits for radar and communications; and sensors and controls for cleaner-burning, more fuel-efficient jet aircraft and automobile engines.

Silicon carbide occurs in many different crystal structures, called polytypes. Despite the fact that all SiC polytypes chemically consist of carbon atoms covalently bonded with equal numbers of silicon atoms, each SiC polytype has its own distinct set of electrical semiconductor properties. While there are more than 100 known polytypes of SiC, only two of them are commonly grown and commercially available in a form acceptable for use as an electronic semiconductor. Both of these polytypes, denoted 4H-SiC and 6H-SiC, respectively, have hexagonal crystal structure. Another polytype, denoted 3C-SiC, has cubic crystal structure and, with respect to use in electronic devices, offers significant benefits over conventional hexagonal SiC polytypes. However, all previous attempts to reproducibly grow 3C-SiC layers have yielded inferior crystals with high densities of defects that make the crystals unusable for realizing their beneficial electronic properties.

Recently, a growth process denoted step-free surface heteroepitaxy has been shown to produce greatly improved 3C-SiC single-crystal films that should enable the reproducible realization of the beneficial properties of 3C-SiC for electronic devices. In this process, the 3C-SiC films are produced on arrays of mesa surfaces that are patterned into commercially available hexagonal-SiC wafers. Figure 1 depicts the subprocesses that affect a mesa. First, reactive-ion etching is performed to form a pattern of trenches into the surface of the

wafer, thereby forming the mesas as the unetched surface areas between trenches. The cross section at the top of Figure 1 shows tightly bonded Si-C bilayers along the crystallographic basal plane, along with single bilayer height steps on the mesa surface that arise because of an unavoidable tilt angle (typically about 0.1°) that is attributable to polishing of the crystal surface at the wafer factory.

Next, pure step-flow homoepitaxy, wherein new reactants become incorporated into the crystal only at the surface steps (which are sites favorable to bond-

ing), is used to grow 4H-SiC from the surface steps on top of each mesa over to the edge of the mesa. Upon completion of this subprocess, the top surface of the mesa is free of atomic steps. That fact that all growth takes place at the steps enables replication of the hexagonal crystal structure of the substrate in this initial epilayer.

After the step-free basal-plane mesa surface of the hexagonal SiC crystal has been established, heteroepitaxial growth of a film having the cubic SiC crystal structure is then initiated by lowering the growth temperature. The lower growth tempera-

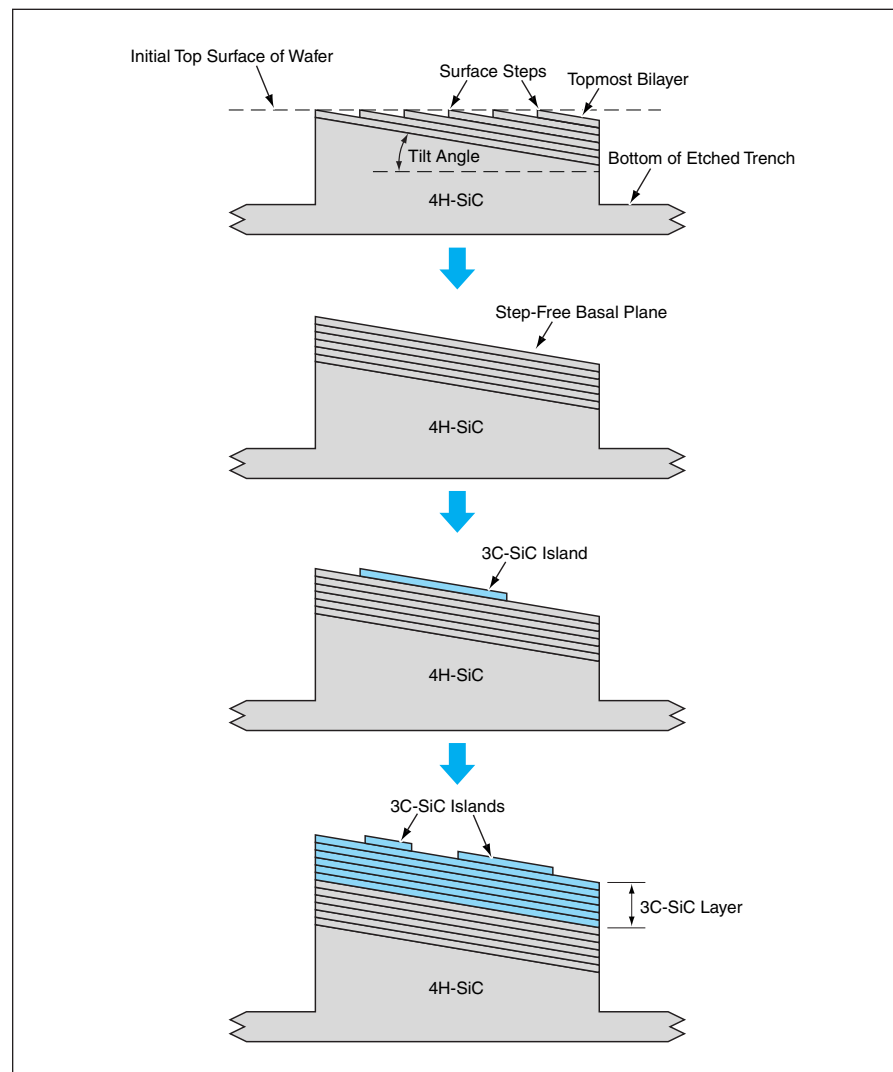


Figure 1. These Schematic Cross Sections of a mesa on a hexagonal-SiC wafer depict the process of growing 3C-SiC by step-free surface heteroepitaxy.

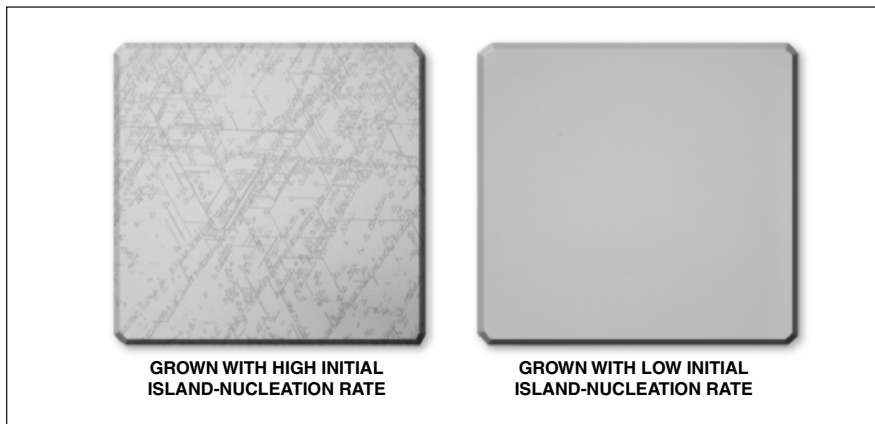


Figure 2. 3C-SiC Films were grown on flattened mesas, then thermally oxidized to reveal crystal defects. The defect-free film shown on the right was made by use of step-free surface heteroepitaxy.

ture enables the growth of 3C-SiC on the basal plane via nucleation of 3C-SiC islands, followed by lateral step-flow expansion. Well-behaved thermodynamic control of polytype occurs in the absence of surface steps, so that the film grows in the cubic crystal structure rather than a hexagonal crystal structure. In experiments, the step-free interface between the hexagonal and cubic polytypes was found to eliminate the double-positioning boundary defects commonly found in previous 3C-SiC heterofilms. However, it was also discov-

ered that the initial 3C-SiC bilayers must be nucleated slowly to obtain 3C-SiC films free of stacking-fault defects.

Figure 2 shows two 0.2-by-0.2-mm mesas topped with 3C-SiC films nearly 2 μm thick and thermally oxidized to reveal stacking-fault defects. As indicated in the figure, the mesas were grown with different initial island-nucleation rates. It has been suggested that what is needed during the initial stages of growth to obtain a defect-free 3C-SiC film is the single-island growth mode, in which a single 3C island nucle-

ates and expands laterally to cover the mesa before a second interfering 3C island nucleates. It has been further suggested that the multiple-island growth mode, depicted at the bottom of the figure, is acceptable after the initial bilayers of the 3C-SiC film have been grown in the single-island mode. In experiments, it was found that 4H-SiC/3C-SiC atomic lattice spacing mismatch was at least partially relieved, without generating stacking faults that threaded to the surface of the film.

The step-free surface heteroepitaxy process is believed to be applicable to growth of heterofilms of materials other than 3C-SiC. Further growth and characterization experiments are in progress, including experiments on the fabrication of prototype 3C-SiC devices and attempting step-free surface heteroepitaxy of GaN films on 4H- or 6H-SiC substrates.

This work was done by Philip G. Neudeck and J. Anthony Powell of Glenn Research Center. Further information is contained in a TSP (see page 1).

Inquiries concerning rights for the commercial use of this invention should be addressed to NASA Glenn Research Center, Commercial Technology Office, Attn: Steve Fedor, Mail Stop 4-8, 21000 Brookpark Road, Cleveland, Ohio 44135. Refer to LEW-17186.

Nonlinear Thermoelastic Model for SMAs and SMA Hybrid Composites

This model captures essential mechanics with fundamental engineering property input.

Langley Research Center, Hampton, Virginia

A constitutive mathematical model has been developed that predicts the nonlinear thermomechanical behaviors of shape-memory alloys (SMAs) and of shape-memory-alloy hybrid composite (SMAHC) structures, which are composite-material structures that contain embedded SMA actuators. SMAHC structures have been investigated for their potential utility in a variety of applications in which there are requirements for static or dynamic control of the shapes of structures, control of the thermoelastic responses of structures, or control of noise and vibrations. The present model overcomes deficiencies of prior, overly simplistic or qualitative models that have proven ineffective or intractable for engineering of SMAHC structures. The model is sophisticated enough to capture the essential features of the mechanics of SMAHC structures yet simple enough to accommodate input from fun-

damental engineering measurements and is in a form that is amenable to implementation in general-purpose structural analysis environments.

SMAs exhibit thermoelastic martensitic transformations. The interaction of temperature and stress applied to an SMA can be used to exploit the shape-memory effect. An SMA can easily be deformed in the low-temperature (martensitic) state and, if not mechanically constrained or restrained, can be returned to its original shape and size by heating through its reverse-transformation temperature range; recovery in this mode is denoted free recovery. If recovery of the original size and shape is completely prevented by mechanical constraint, then the heating results in a large stress and the recovery is said to be constrained. If the SMA is neither completely free nor constrained but, instead, disposed to perform work by deforming under load, then the

recovery is said to be restrained.

The model expresses the nonlinear thermoelastic nature of an SMA in the form of an effective coefficient of thermal expansion (CTE). This form enables representation of shape-memory behavior, on the basis of either (1) measurement of the effective CTE or (2) inference of thermal strain from measured values of the recovery stress and the modulus of elasticity. The model captures the thermoelastic nonlinearity of the SMA implicitly and provides a simple means of including nonlinear thermoelastic effects of a matrix material in an SMAHC structure. The model can predict constrained and free recovery implicitly and the combination of this model with a model of nonlinear elasticity can predict restrained recovery.

The constitutive equations for a given SMA, SMAHC, or a larger structure that incorporates an SMAHC as a substructure

can be derived, using the present model as a basis, following a mechanics-of-materials approach or other suitable approach. The present constitutive model, in combination with classical lamination theory, has been incorporated into a finite-element mathematical model and computer code to enable modeling of static and dynamic responses of panel-type SMAHC structures subjected to static and dynamic

thermal and mechanical loads. Loads that have been considered include acoustic pressures, acceleration forces, and concentrated forces. Phenomena that have been investigated include control of thermal buckling, thermal post-buckling, random vibration, and acoustic transmission/radiation responses of structures under constrained recovery. The constitutive model and structural response for-

mulation have been validated against experimental measurements of thermal buckling/post-buckling and random vibration responses.

This work was done by Travis L. Turner of Langley Research Center. For further information, access the Technical Support Package (TSP) free on-line at www.techbriefs.com/tsp under the Materials category. LAR-16274

Liquid-Crystal Thermosets, a New Generation of High-Performance Liquid-Crystal Polymers

Liquid-crystal polymers can now be used as resins in textile composites.

Langley Research Center, Hampton, Virginia

One of the major challenges for NASA's next-generation reusable-launch-vehicle (RLV) program is the design of a cryogenic lightweight composite fuel tank. Potential matrix resin systems need to exhibit a low coefficient of thermal expansion (CTE), good mechanical strength, and excellent barrier properties at cryogenic temperatures under load. In addition, the resin system needs to be processable by a variety of non-autoclavable techniques, such as vacuum-bag curing, resin-transfer molding (RTM), vacuum-assisted resin-transfer molding (VaRTM), resin-film infusion (RFI), pultrusion, and advanced tow placement (ATP).

To meet these requirements, the Advanced Materials and Processing Branch (AMPB) at NASA Langley Research Center developed a new family of wholly aromatic liquid-crystal oligomers that can be processed and thermally cross-linked while maintaining their liquid-crystal order. All the monomers were polymerized in the presence of a cross-linkable unit by use of an environmentally benign melt-condensation technique. This method does not require hazardous solvents, and the only side product is acetic acid. The final product can be obtained as a powder or granulate and has an infinite shelf life. The obtained oligomers melt into a nematic phase and do not exhibit isotropization temperatures greater than the temperatures of decomposition ($T_i > T_{dec}$). Three aromatic formulations were designed and tested and included esters, ester-amides, and ester-imides.

One of the major advantages of this invention, named LaRC-LCR or Langley Research Center-Liquid Crystal Resin, is the ability to control a variety of resin characteristics, such as melting temperature, vis-

cosity, and the cross-link density of the final part. Depending on the formulation, oligomers can be prepared with melt viscosities in the range of 10–10,000 poise (100 rad/s), which can easily be melt-processed using a variety of composite-processing techniques. This capability provides NASA with custom-made matrix resins that meet the required processing conditions for the fabrication of textile composites. Once the resin is in place, the temperature is raised to 375 °C and the oligomers are cross-linked into a high-glass-transition-temperature (T_g) nematic network without releasing volatiles. The mechanical properties of the fully cross-linked, composite articles are comparable to typical composites based on commercially available epoxy resins.

LaRC-LCR can also be used in thermoforming techniques where short holding times are desired. The resin can be used to spin fibers, extrude thin films and sheets, or injection mold complex parts. Although LaRC-LCR has been developed to meet NASA's needs towards the development of a next-generation launch vehicle, other applications can be envisioned as well. The thermal and mechanical behavior of this material are ideally suited for electronic applications and may find use in flexible circuits, chip housings, and flip-chip underfills. Another area where thermal stability and chemical resistance are highly desirable is the automotive industry. Distributor caps, fuel tanks, air-intake manifolds, rocker covers, and ignition systems

are among the potential applications. The low viscosity of this resin makes this material ideal for coating applications as well. Fine powders have been used in plasma-spray applications, and well-defined thin coatings were obtained. LaRC-LCR can also be used as an adhesive. Lap-shear values of 3,435 psi (22,683 kPa) were easily obtained. In contrast, these values are ≈ 20 times higher than those observed in commercially available LCP resins.

This work was done by Theo Dingemans, Erik Weiser, Tan Hou, Brian Jensen, and Terry StClair at Langley Research Center and funded under NASA's Reusable Launch Vehicle (RLV) research program.

This invention is owned by NASA, and a patent application has been filed. An exclusive license for its commercial development has been granted to TICONA Inc. (Summit, NJ). For further information, contact Diane Hope at the Technology Commercialization Program Office (TCPO), NASA Langley Research Center, 3 Langley Boulevard, Mail Stop 200, Hampton, VA 23681-2199. E-mail: d.l.hope@larc.nasa.gov. LAR-16079



Several Products made from LaRC-LCR include films, plaques, foams, uniaxial carbon-fiber prepregs, and carbon-fiber composites.

Formulations for Stronger Solid Oxide Fuel-Cell Electrolytes

Alumina is added to yttria-stabilized zirconia.

John H. Glenn Research Center, Cleveland, Ohio

Tests have shown that modification of chemical compositions can increase the strengths and fracture toughnesses of solid oxide fuel-cell (SOFC) electrolytes. Heretofore, these solid electrolytes have been made of yttria-stabilized zirconia, which is highly conductive for oxygen ions at high temperatures, as needed for operation of fuel cells. Unfortunately yttria-stabilized zirconia has a high coefficient of thermal expansion, low resistance to thermal shock, low fracture toughness, and low mechanical strength. The lack of strength and toughness are especially problematic for fabrication of thin SOFC electrolyte membranes needed for contemplated aeronautical, automotive, and stationary power-generation applications.

The modifications of chemical composition that lead to increased strength and fracture toughness consist in addition of

alumina to the basic yttria-stabilized zirconia formulations. Techniques for processing of yttria-stabilized zirconia/alumina composites containing as much as 30 mole percent of alumina have been developed. The composite panels fabricated by these techniques have been found to be dense and free of cracks. The only material phases detected in these composites has been cubic zirconia and a alumina: this finding signifies that no undesired chemical reactions between the constituents occurred during processing at elevated temperatures.

The flexural strengths and fracture toughnesses of the various zirconia-alumina composites were measured in air at room temperature as well as at a temperature of 1,000 °C (a typical SOFC operating temperature). The measurements showed that both flexural

strength and fracture toughness increased with increasing alumina content at both temperatures. In addition, the modulus of elasticity and the thermal conductivity were found to increase and the density to decrease with increasing alumina content. The oxygen-ion conductivity at 1,000 °C was found to be unchanged by the addition of alumina.

*This work was done by Narottam P. Bansal and John C. Goldsby of **Glenn Research Center** and Sung R. Choi of Ohio Aerospace Institute. Further information is contained in a TSP (see page 1).*

Inquiries concerning rights for the commercial use of this invention should be addressed to NASA Glenn Research Center, Commercial Technology Office, Attn: Steve Fedor, Mail Stop 4-8, 21000 Brookpark Road, Cleveland, Ohio 44135. Refer to LEW-17380.



Simulation of Hazards and Poses for a Rocker-Bogie Rover

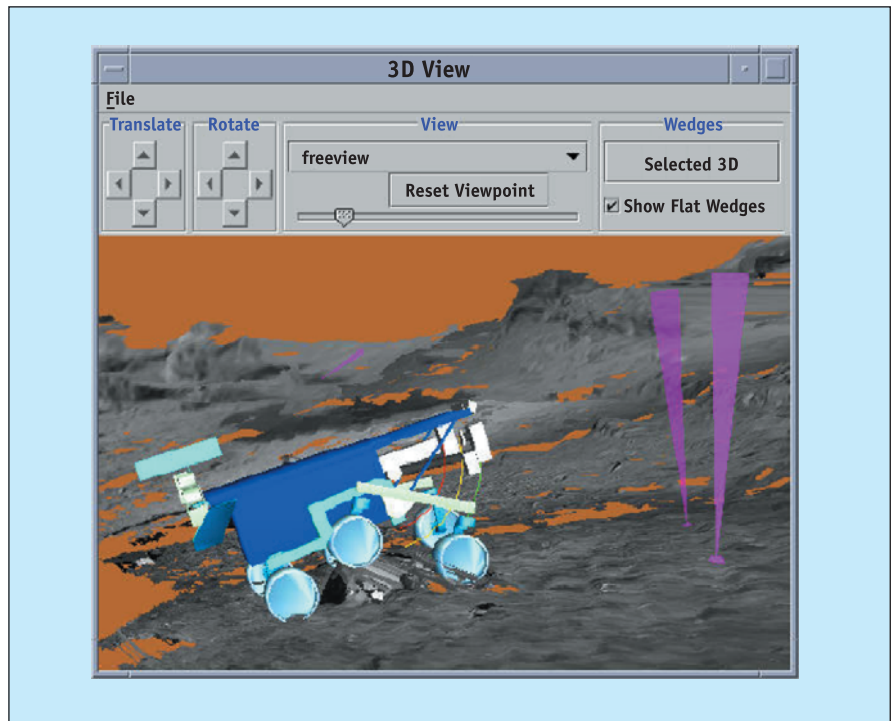
Vehicle poses and locations of hazards can be viewed before attempting traverses.

NASA's Jet Propulsion Laboratory, Pasadena, California

Provisions for specification of hazards faced by a robotic vehicle (rover) equipped with a rocker-bogie suspension, for prediction of collisions between the vehicle and the hazards, and for simulation of poses of the vehicle at selected positions on the terrain have been incorporated into software that simulates the movements of the vehicle on planned paths across the terrain. The software in question is that of the Web Interface for Telescience (WITS), selected aspects of which have been described in a number of prior *NASA Tech Briefs* articles. To recapitulate: The WITS is a system of computer software that enables scientists, located at geographically dispersed computer terminals connected to the World Wide Web, to command instrumented robotic vehicles (rovers) during exploration of Mars and perhaps eventually of other planets. The WITS also has potential for adaptation to terrestrial use in telerobotics and other applications that involve computer-based remote monitoring, supervision, control, and planning.

The hazard-specification provision enables a user to interactively specify hazards in terms of zones on the terrain. On an interactive computer display that contains an overhead view synthesized from previously acquired images of the terrain, the user specifies the horizontal location of the center of a hazard zone. Then, using a display denoted a hazard window, the user specifies the height of the center of the hazard zone and the horizontal radius of the hazard zone. The user can also add a textual comment about the hazard. Once the hazard zone has been thus specified, it is depicted as a yellow circle on WITS synthetic views of the terrain.

The collision-prediction provision enables a user to see where the planned rover path could cause the rover to collide with a specified hazard. The traversal of the terrain by the rover is specified by designating way points, and the planned path becomes a sequence of straight-line (as viewed from overhead) segments between the way points. At small increments of position along the planned path, the distance from the rover to all the speci-



This **Computer-Generated Image** is typical of the images generated in simulations of the articulation of the rocker bogies and the tilt of the main body of the rover as it traverses terrain.

fied hazard zones is computed. The difference between each such distance and the radius of the hazard zone is computed and compared with two previously specified distances: one denoted the safe distance and a smaller one denoted the collision distance. If the computed difference distance exceeds the safe distance, then there is assumed to be no risk of collision and the affected segment of the path is shown green on the WITS synthetic terrain images. If the computed difference distance lies between the safety and collision distances, the affected path segment is deemed to be risky and is shown yellow on the terrain images. If the computed difference distance is less than the collision distance, the affected path segment is designated as a collision segment and is displayed in red.

The pose-simulation provision is, more specifically, a provision for simulating the articulation of the rocker-bogie portions of the suspension and the tilt of the main body of the vehicle, given the equivalent

of a topographical map of the local terrain with which the vehicle is in contact (see figure). This provision enables the user to view the changing rover bogie angles as the rover travels its planned path across the terrain. For each increment of position along the path, the horizontal positions of the six rover wheels are computed approximately under the assumption that the rover tilt angles are small. Then the elevations of the wheels are computed by use of the estimated horizontal wheel coordinates and the topographical information. Then the bogie angles and the tilt angles of the main body are determined from the elevations of the wheels and the known geometric relationships among the wheels, the bogies, and the main body.

This work was done by Paul Backes, Jeffrey Norris, and Mark Powell of Caltech and Gregory Tharp of IA Tech, Inc., for NASA's Jet Propulsion Laboratory. Further information is contained in a TSP (see page 1). NPO-30450

Autonomous Formation Flight

A primary goal is to reduce fuel consumption during cruise by 10 percent.

Dryden Flight Research Center, Edwards, California

NASA's Strategic Plan for the Aerospace Technology Enterprise includes ambitious objectives focused on affordable air travel, reduced emissions, and expanded aviation-system capacity. NASA Dryden Flight Research Center, in cooperation with NASA Ames Research

Center, the Boeing Company, and the University of California, Los Angeles, has embarked on an autonomous-formation-flight project that promises to make significant strides towards these goals.

For millions of years, birds have taken advantage of the aerodynamic benefit of

flying in formation. The traditional "V" formation flown by many species of birds (including gulls, pelicans, and geese) enables each of the trailing birds to fly in the upwash flow field that exists just outboard of the bird immediately ahead in the formation. The result for each trailing bird is a decrease in induced drag and thus a reduction in the energy needed to maintain a given speed. Hence, for migratory birds, formation flight extends the range of the system of birds over the range of birds flying solo. The Autonomous Formation Flight (AFF) Project is seeking to extend this symbiotic relationship to aircraft (see Figure 1).

Predicted benefits of AFF as applied to commercial transport airplanes for typical transcontinental routes include annual per-trailing-airplane reductions of $\$0.5 \times 10^6$ (year 2000 average prices) in the cost of fuel, 10^7 lb ($\approx 4.5 \times 10^6$ kg) in emitted carbon dioxide, and 10^5 lb ($\approx 4.5 \times 10^4$ kg) in emitted nitrous oxide. In addition, improvements in cooperative guidance and control could one day enable air-traffic-control systems to manage formations of aircraft as though they were single aircraft, thereby increasing overall throughput.

AFF was competitively selected in May 2000 by the Revolutionary Concepts in Aeronautics (RevCon) project, funded under Dryden Flight Research Centers's R&T Base Program. RevCon was designed to accelerate, through flight research, the dissemination of new aircraft and system concepts.

The primary goal of the AFF project is to demonstrate a sustained 10-percent reduction in the consumption of fuel by a trailing airplane during cruise. The project intends to advance the concept of autonomous-formation-flight drag reduction from the experimental proof-of-concept stage to a prototype demonstration within three years. The prototype demonstration will be accomplished by use of two highly instrumented NASA F/A-18 aircraft equipped with the necessary research systems.

The AFF project will involve three phases, with flight tests beginning in the first quarter of fiscal year 2001 and completion by the end of fiscal year 2003. The first phase, which has taken place, was devoted to the demonstra-



Figure 1. Formation Flight offers the advantage of reduced overall drag for both birds and airplanes.

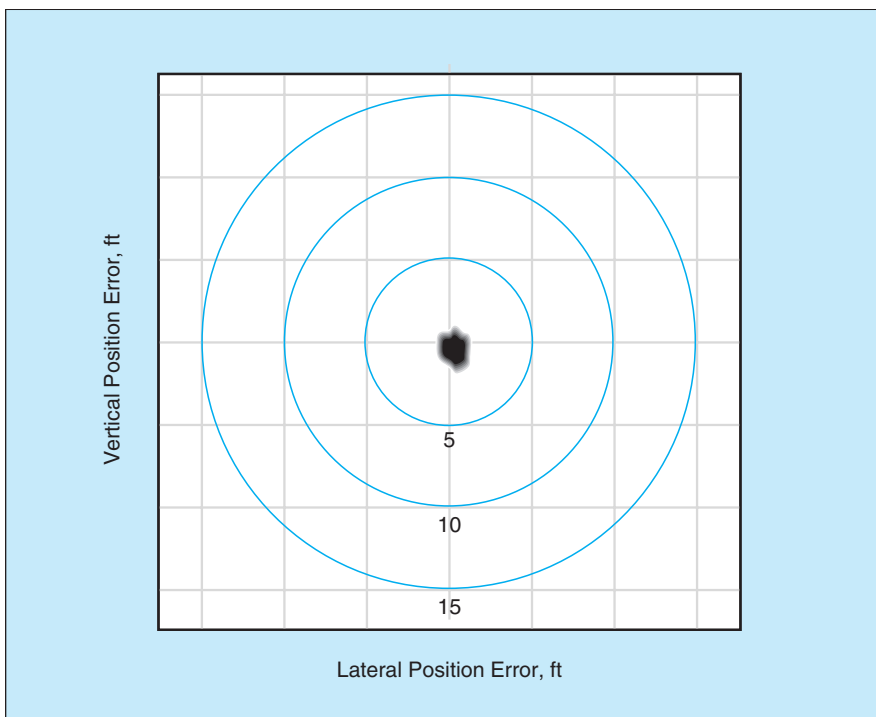


Figure 2. The **Narrowness of the Scatter** of relative-position measurements taken in flight tests is proof of the viability of a formation autopilot system.

tion of precise autonomous station keeping. The second phase, also completed, involved mapping of the effects of leading-airplane-generated vortices on a evaluation of the performances of a highly accurate relative-position-sensing system and of a data-link system. The primary goal of the project — demonstration of integrated system performance, including a sustained 10-percent reduction in fuel consumption in close, autonomous formation flight — will be reached in the third phase. The results of this phase will be applicable to commercial and military cargo and passenger transport aircraft, unpiloted aircraft, increasing the ranges of aircraft in general, aerial refueling and resupply, and formation flying of satellites.

The AFF project is developing the first system for highly accurate in-flight relative positioning of two aircraft to incorporate differential-carrier-phase Global Positioning System (GPS) and inertial measurement information with an extended Kalman filter in a moving-base-station scenario. This system is expected to yield relative-position measurements accurate to within 0.5 ft (0.15 m). Flight tests will enable evaluation of control-system approaches and performance, validation of mathematical models for predicting vortex effects, quantification of reductions of drag,

and evaluation of operational effectiveness. The flight tests will provide insight into such phenomena as effects of multipath propagation on GPS measurements and data communications and the dynamics of (including interactions between) vortices that cannot be adequately identified through simulation or ground test.

During the first phase of the program, two F/A-18 airplanes were outfitted with identical GPS receivers and an air-to-air telemetry system as a data link between the airplanes. In addition, the trailing airplane was equipped with an airborne research test system (ARTS) and a research flight-control computer. The ARTS hosted a precise autopilot control system, which received GPS and inertial measurement data from the leading airplane and computed stick commands to place the trailing airplane at the desired relative position. The research flight-control computer received and used the stick commands from the ARTS while engaged, but reverted to the production F-18 flight control system for the remainder of the mission. An interactive display was installed in the back seat of the airplane to enable the flight crew to control the flight experiment. Lateral and vertical position errors were displayed to the pilot by use of instrument-landing-system needles.

A standard test block of six maneuvers was repeated for each of four different autopilot gain sets. These maneuvers included five-minute steady-state tracking tests and 30-ft (≈ 9 -m) commanded step inputs in each axis. The dynamic response of the system was observed in maneuvers in which the leading airplane performed heading sweeps of a few degrees and altitude sweeps of several hundred feet (≈ 100 m).

A total of 167 tests points was reached in 11 research flights. The experiment met all project objectives. The formation autopilot maintained relative position to within 2 ft (0.61 m) [see Figure 2] for all four gain sets during straight and level flight with turbulence levels ranging from nonexistent to light chop. An additional position error of up to 3 ft (0.91 m), due to GPS navigation errors, brought the total formation position error to less than 5 ft (1.52 m). Accurate, predictable tracking was observed during the step and dynamic maneuvers.

This work was done by Gerard S. Schkolnik and Brent Cobleigh of Dryden Flight Research Center. For more information on the AFF project contact Gerard S. Schkolnik, AFF Project Manager, gerard.schkolnik@dfrc.nasa.gov, (661) 276-3055 or Brent Cobleigh, AFF Chief Engineer, brent.cobleigh@dfrc.nasa.gov, (661) 276-2249. DRC-01-46

Expandable Purge Chambers Would Protect Cryogenic Fittings

Flowing dry nitrogen would prevent accumulation of ice or airborne particles.

John F. Kennedy Space Center, Florida

Expandable ice-prevention and cleanliness-preservation (EIP-CP) chambers have been proposed to prevent the accumulation of ice or airborne particles on quick-disconnect (QD) fittings, or on ducts or tubes that contain cryogenic fluids. In the original application for which the EIP-CP chambers were conceived, there is a requirement to be able to disconnect and reconnect the QD fittings in rapid succession. If ice were to form on the fittings by condensation and freezing of airborne water vapor on the cold fitting surfaces, the ice could interfere with proper mating of the fittings, making it necessary to wait an unacceptably long time for the ice to thaw before attempting reconnection. By keeping water vapor away from the cold fitting surfaces, the EIP-CP chambers

would prevent accumulation of ice, preserving the ability to reconnect as soon as required.

Basically, the role of an EIP-CP chamber would be to serve as an enclosure for a flow of dry nitrogen gas that would keep ambient air away from QD cryogenic fittings. An EIP-CP chamber would be an inflatable device made of a fabric-like material. The chamber would be attached to an umbilical plate holding a cryogenic QD fitting. The chamber would include inner and outer subchambers that would be inflated with gaseous nitrogen through separate supply tubes. The outer subchamber would resemble a small tire tube. The inner chamber would be perforated on its innermost circle to allow nitrogen to flow onto and around the QD surfaces. When

deflated, the EIP-CP would be about 1 in. (≈ 2.5 cm) thick.

When not in use, the EIP-CP would be kept deflated, flat against the umbilical plate. Before disconnecting the QD fitting, the two subchambers of the EIP-CP would be pressurized with nitrogen. As disconnection proceeded, the pressurized outer tube would expand to follow the moving umbilical plate of the mating fitting, up to a maximum axial thickness (corresponding to a tire width) of about 6 in. (≈ 15 cm). The subchambers would be shaped so that once maximum expansion was reached and the chamber could no longer seal against the receding umbilical plate of the mating fitting, the opening on the exposed end of the chamber would narrow to a small hole. The purge flow of

nitrogen would keep ambient air out of the chamber.

To prepare for reconnection, the umbilical plate of the mating fitting would be brought into contact with the EIP-CP chamber and the supply of nitro-

gen would be turned off. Then a vacuum pump would be used to deflate the nitrogen from the outer chamber, so that the chamber could be pressed flat against its umbilical plate and the mating QD connectors pushed together.

This work was done by Ivan I. Townsend III of Dynacs, Inc., For further information contact the Technology Programs and Commercialization Office at (321) 867-8130 for Kennedy Space Center. KSC-12460

Wavy-Planform Helicopter Blades Make Less Noise

Improved designs reduce strengths of BVI-noise and thickness-noise sources.

Langley Research Center, Hampton, Virginia

Wavy-planform rotor blades for helicopters have been investigated for the first time in an effort to reduce noise. Two of the main sources of helicopter noise are blade/vortex interaction

(BVI) and volume displacement. (The noise contributed by volume displacement is termed thickness noise.) The reduction in noise generated by a wavy-planform blade, relative to that

generated by an otherwise equivalent straight-planform blade, affects both main sources: (1) the BVI noise is reduced through smoothing and defocusing of the aerodynamic loading on the blade and (2) the thickness noise is reduced by reducing gradients of thickness with respect to listeners on the ground.

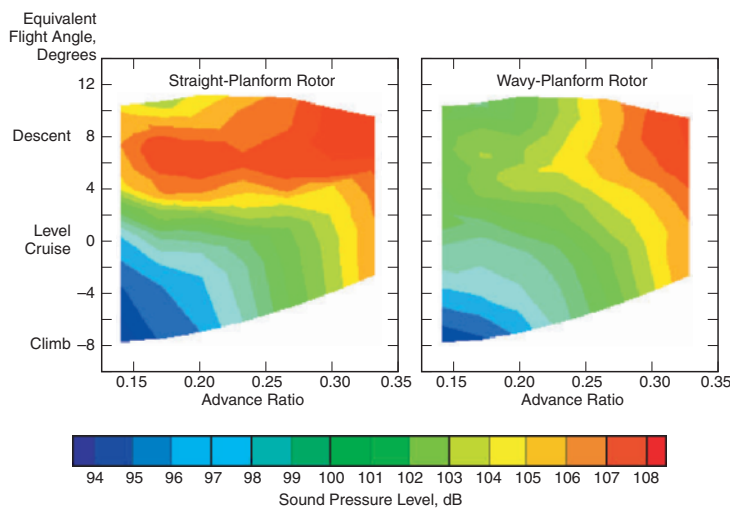
Noise tests were performed in a reverberant wind tunnel on a model helicopter (see photo). In the tests, sound-pressure levels were measured over a range of flight angles and advance ratios (the advance ratio is defined as the ratio between the horizontal speed of a helicopter and the speed of the tip of a rotor blade). Sound-pressure levels were also measured under the same conditions using a baseline rotor that had a rectangular-planform blade with linear twist.

The figure presents color contour plots of some of the data from the tests. These plots show that during descent (landing) flight conditions, which are most strongly dominated by BVI noise, sound-pressure levels of the wavy-planform blades were more than 4 dB below those of the rectangular planform blades. Some mild reduction in noise was also found for other flight conditions of climb and level cruise over all frequency ranges. Further testing and analysis of data will be needed to further quantify reduction of noise, vibration, and performance benefits, leading eventually to refinements in the designs of wavy-planform blades.

This work was done by Thomas F. Brooks of Langley Research Center. For further information, contact the Langley Commercial Technology Office at (757) 864-3936. LAR-16084



Wavy-Planform Rotor on Model Helicopter in Wind Tunnel



Wavy-Planform Rotor Blades on a model helicopter in a reverberant wind tunnel were found to generate less noise than did rectangular-planform blades.



Miniature Robotic Spacecraft for Inspecting Other Spacecraft

Lyndon B. Johnson Space Center, Houston, Texas

A report discusses the Miniature Autonomous Extravehicular Robotic Camera (Mini AERCam) — a compact robotic spacecraft intended to be released from a larger spacecraft for exterior visual inspection of the larger spacecraft. The Mini AERCam is a successor to the AERCam Sprint — a prior miniature robotic inspection spacecraft that was demonstrated in a space-shuttle flight experiment in 1997. The prototype of the Mini AERCam is a demonstration unit having approximately the form and function of a flight system. The Mini AERCam is approximately spher-

ical with a diameter of about 7.5 in. (≈ 19 cm) and a weight of about 10 lb (≈ 4.5 kg), yet it has significant additional capabilities, relative to the 14-in. (36-cm), 35-lb (16-kg) AERCam Sprint. The Mini AERCam includes miniaturized avionics, instrumentation, communications, navigation, imaging, power, and propulsion subsystems, including two digital video cameras and a high-resolution still camera. The Mini AERCam is designed for either remote piloting or supervised autonomous operations, including station keeping and point-to-point maneuvering. The prototype has

been tested on an air-bearing table and in a hardware-in-the-loop orbital simulation of the dynamics of maneuvering in proximity to the International Space Station.

This work was done by Steven Fredrickson, Larry Abbott, Steve Duran, Robert Goode, Nathan Howard, David Jochim, Steve Rickman, Tim Straube, Bill Studak, Jennifer Wagenknecht, Matthew Lemke, Randall Wade, Scott Wheeler, and Clinton Baggerman of Johnson Space Center. Further information is contained in a TSP (see page 1).MSC-23669

Miniature Ring-Shaped Peristaltic Pump

Piezoelectrically excited fluid-transport volumes travel around a ring.

NASA's Jet Propulsion Laboratory, Pasadena, California

An experimental miniature peristaltic pump exploits piezoelectrically excited flexural waves that travel around a ring: A fluid is carried in the containers formed in the valleys between the peaks of the flexural waves (see Figure 1). The basic

action of this pump is similar to that described in "Piezoelectric Flexural-Traveling-Wave Pumps" (NPO-19737), *NASA Tech Briefs*, Vol. 21, No. 4 (April 1997), page 66.

What sets the present pump apart

from other pumps that exploit piezoelectrically excited flexural waves is the ring shape, which makes it possible to take advantage of some of the desirable characteristics of previously developed piezoelectric rotary motors. A major advantage of the circular (in contradistinction to a straight-line) wave path is that the flexural waves do not come to a stop and, instead, keep propagating around the ring. Hence, a significant portion of the excitation energy supplied during each cycle is reused during the next cycle, with the result that the pump operates more effectively than it otherwise would.

The principal components of this pump (see Figure 2) include a cover and segmented-ring piezoelectric actuator bonded to one face of a brass ring. The other face of the brass ring is pressed against the cover and against silicone rubber seals that protrude slightly from grooves in the cover. The protrusion is sufficient to maintain sealing at the maximum flexural-wave amplitude expected to occur during operation of the pump. The pattern of grooves and seals is chosen, in conjunction with the pattern of inlet and outlet holes in the

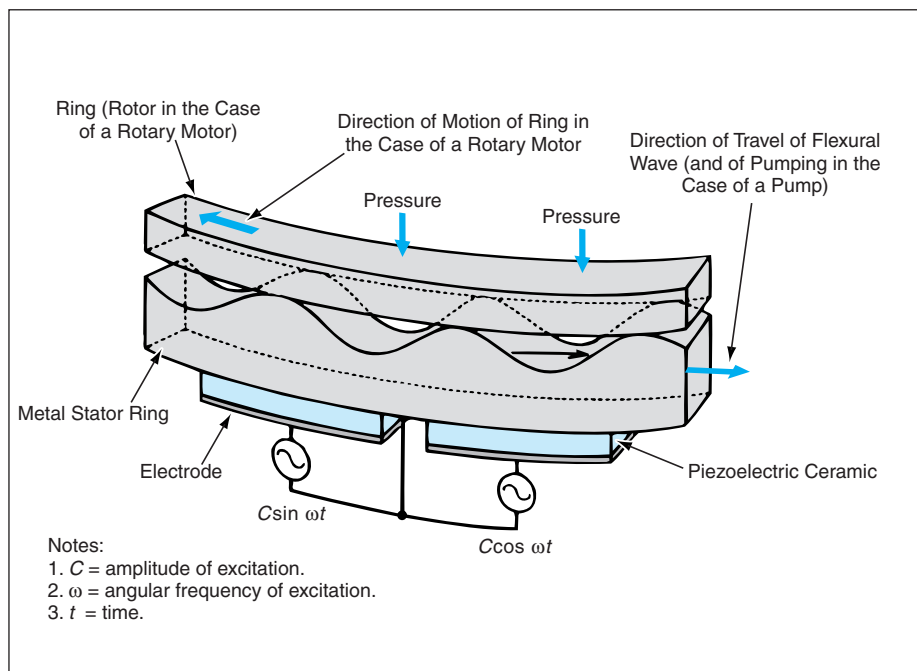


Figure 1. **Traveling Flexural Waves** similar to those in a piezoelectric rotary motor are exploited for pumping. Fluid is carried around a circle in the troughs of the waves.

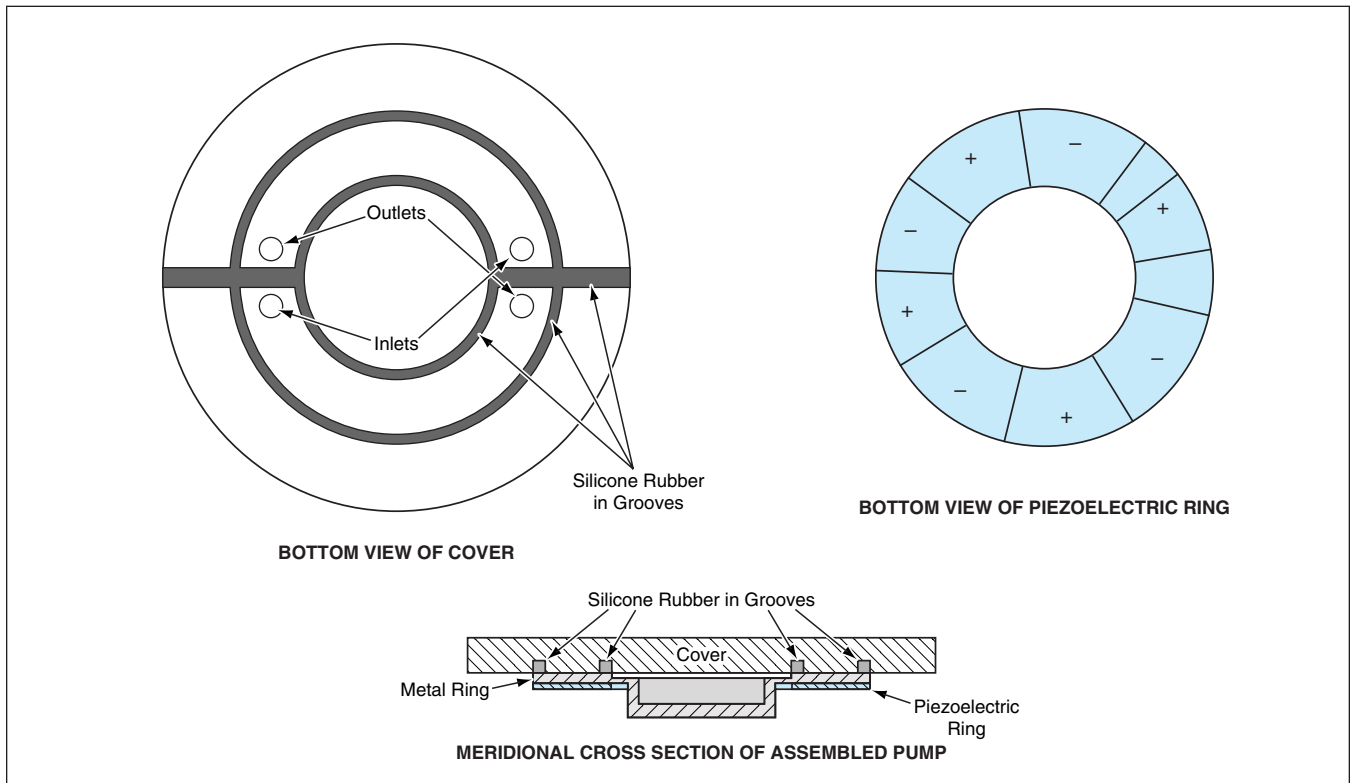


Figure 2. The Ring-Shaped Peristaltic Pump features components designed to maximize the pumping effect depicted in Figure 1.

cover, to eliminate the need for conventional valve mechanisms, sliding seals, and other moving parts that would be highly susceptible to wear. Moreover, when the pump is turned off (that is, in the absence of piezoelectrically actuated flexural waves), the loading of the brass ring against the cover effects a tight seal equivalent to that of a closed valve.

The polarities and phases of the voltages applied to the piezoelectric ring segments are chosen to excite a desired

flexural-traveling-wave mode. For maximum pumping effectiveness, the excitation frequency should equal the resonance frequency of the desired wave mode.

This work was done by Yoseph Bar-Cohen, Zensheu Chang, Xiaoqi Bao, and Shyh-Shiuh Lih of Caltech for NASA's Jet Propulsion Laboratory. Further information is contained in a TSP (see page 1).

In accordance with Public Law 96-517, the contractor has elected to retain title to this

invention. Inquiries concerning rights for its commercial use should be addressed to:

*Intellectual Assets Office
JPL*

*Mail Stop 202-233
4800 Oak Grove Drive
Pasadena, CA 91109
(818) 354-2240*

E-mail: ipgroup@jpl.nasa.gov

Refer to NPO-30415, volume and number of this NASA Tech Briefs issue, and the page number.

⚙️ Compact Plasma Accelerator

Applications could include processing of materials and propulsion of spacecraft.

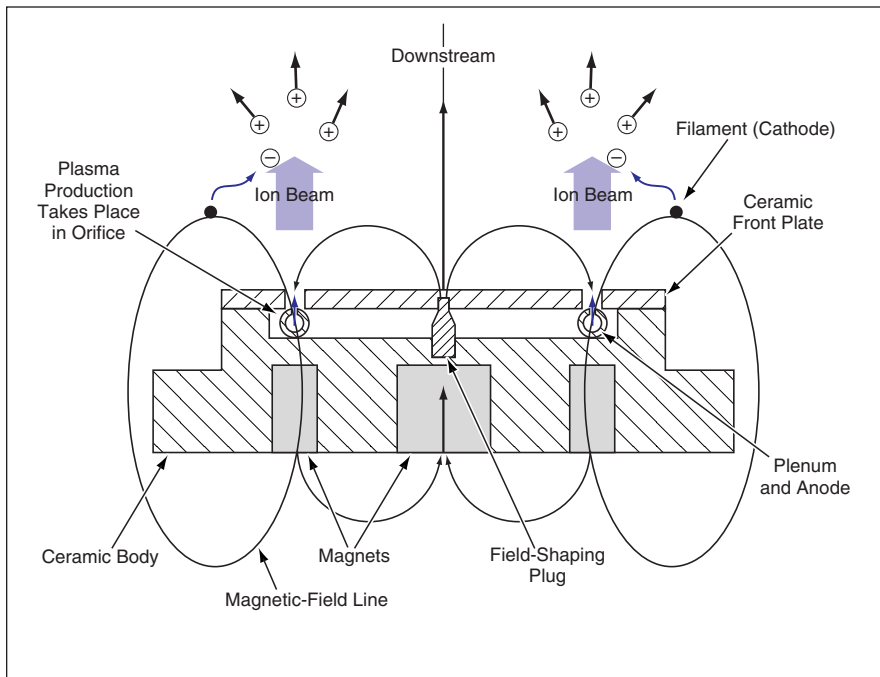
John H. Glenn Research Center, Cleveland, Ohio

A plasma accelerator has been conceived for both material-processing and spacecraft-propulsion applications. This accelerator generates and accelerates ions within a very small volume. Because of its compactness, this accelerator could be nearly ideal for primary or station-keeping propulsion for spacecraft having masses between 1 and 20 kg. Because this accelerator is designed to generate beams of ions having energies between 50 and 200 eV, it could also be used for surface modification or activation of thin films.

The figure illustrates selected aspects of this accelerator. A propellant gas is injected through a feed plenum that is perforated with openings that constitute capillarylike channels in the following sense: They are narrow enough that even at low flow rates, the pressure in them is sufficiently high [a few Torr (a few hundred pascals)] that the depth of channels (the thickness of the plenum wall) is of the order of electron/neutral-atom mean free path. The plenum, which is at anode potential, is centered

above a magnetic cusp generated by a permanent-magnet circuit that consists of ring of magnets surrounding a central magnet.

The magnetic cusp funnels energetic electrons into the plenum openings. These electrons ionize the propellant gas in the channels. Hence, each plenum orifice serves as a very compact, independent discharge cell that provides copious amounts of ions that are subsequently accelerated by sheath potentials. The plasma-production volume, as estimated



This **Partially Schematic Cross Section** illustrates the design and the principle of operation of the compact plasma accelerator. The device is symmetrical about the z axis.

partly on the basis of the depth of the channels, is of the order of 0.05 mm^3 .

The source of electrons is an annular hot filament. This source is located such that emitted electrons must diffuse across the magnetic field to reach the anode. The transverse component of the magnetic field tends to increase the cathode fall voltage. The increase in the cathode fall voltage is necessary for producing energetic electrons for ionization inside the channels. Energetic electrons that have sufficient velocity components parallel to

the magnetic field enter the channels to participate in the ionization process. Those without sufficient parallel velocities are reflected by the magnetic-mirror force (a consequence of the chosen magnetic-field configuration and strength). Because the electrons reflected by the mirror force are constrained by the magnetic-field lines, the reflected electrons oscillate between the filament and the plenum. The likelihood that these electrons will ionize neutral atoms in the plenum region increases as this oscillation continues.

Ions formed in the channels are accelerated by the electrostatic-potential gradient across the plasma sheath at the plenum. The ions emitted from the sheath at the anode plenum form an axially directed beam. The ion beam is neutralized by electrons emitted into the beam by the filament. In this respect, the filament provides not only the ionizing electrons but also the neutralizing electrons.

It should be pointed out that the choice of the electron source used in this device is quite general. In the prototype, a coated filament was used. The basic concept of this compact plasma accelerator (CPA) is also compatible with a field-emitter-array cathode. The appeal of the field-emitter approach lies in a higher current density and greater simplicity of integration (no filament heater supply is necessary).

A prototype of this CPA generated a monoenergetic (80-eV) ion beam of 30-mA current at a discharge power of approximately 40 W. The propellant efficiency at this condition was calculated to be approximately 88 percent. The peak ion current densities of the beamlets formed in the prototype CPA were similar to those measured in gridded ion thrusters of much higher power (e.g., 2.3 kW).

This work was done by John E. Foster of Glenn Research Center. Further information is contained in a TSP (see page 1).

Inquiries concerning rights for the commercial use of this invention should be addressed to NASA Glenn Research Center, Commercial Technology Office, Attn: Steve Fedor, Mail Stop 4-8, 21000 Brookpark Road, Cleveland, Ohio 44135. Refer to LEW-17230.

Improved Electrohydraulic Linear Actuators

Advantages include better position control and end-of-stroke buffering.

Stennis Space Center, Mississippi

A product line of improved electrohydraulic linear actuators has been developed. These actuators are designed especially for use in actuating valves in rocket-engine test facilities. They are also adaptable to many industrial uses, such as steam turbines, process control valves, dampers, motion control, etc.

The advantageous features of the improved electrohydraulic linear actuators are best described with respect to shortcomings of prior electrohydraulic linear actuators that the improved ones are intended to supplant. The shortcomings are the following:

- They perform unreliably and inconsistently as positioning devices.
- Their capabilities for end-of-stroke buffering (that is, deceleration to gentle stops at designated stopping positions) range from unsatisfactory to nonexistent, with consequent potential for inducing catastrophic failures.
- It takes long times to manufacture special actuators to meet specifications, and the costs of such actuators are high.

The figure depicts one of the improved actuators. The flow of hydraulic fluid to the two ports of the actuator

cylinder is controlled by a servo valve that is controlled by a signal from a servo amplifier that, in turn, receives an analog position-command signal (a current having a value between 4 and 20 mA) from a supervisory control system of the facility. As the position command changes, the servo valve shifts, causing a greater flow of hydraulic fluid to one side of the cylinder and thereby causing the actuator piston to move to extend or retract a piston rod from the actuator body. A linear variable differential transformer (LVDT) directly linked to the piston provides a



This **Electrohydraulic Linear Actuator** incorporates several improvements over prior commercially available devices of a similar nature.

position-feedback signal, which is compared with the position-command signal in the servo amplifier. When the position-feedback and position-command signals match, the servo valve moves to its null position, in which it holds the actuator piston at a steady position.

The actuator includes a deceleration feature for both extremes of the piston stroke. When the actuator is used to open and close a valve, the deceleration feature prevents damage to valve seats and other components during cycles of rapid stroking. Because the resolution of the LVDT is, for practical purposes, unlimited, the position feedback from the LVDT acts, in conjunction with the deceleration feature, to afford maximum protection against damage in those ranges of position in which protection is most needed. Other advantageous features of the improved actuators are the following:

- To eliminate leaks associated with common tubing connections, the components within the actuator that must be

connected to high-pressure hydraulic fluid are connected via a manifold.

- The time and cost of manufacturing are less than those of the prior actuators.
- Optionally, fail-safe valves of a type used widely in the petrochemical industry can be incorporated into the actuators.

This work was done by James Hamtil of BAFCO, Inc., for Stennis Space Center.

In accordance with Public Law 96-517, the contractor has elected to retain title to this invention. Inquiries concerning rights for its commercial use should be addressed to

BAFCO, Inc.

PO Box 2428

717 Mearns Road

Warminster, PA 18974

(215) 674-1700

E-mail: bafco@voicenet.com

Refer to SSC-00165, volume and number of this NASA Tech Briefs issue, and the page number.

⚙️ A Software Architecture for Semiautonomous Robot Control

Lyndon B. Johnson Space Center, Houston, Texas

A software architecture has been developed to increase the safety and effectiveness with which tasks are performed by robots that are capable of functioning autonomously but sometimes are operated under control by humans. The control system of such a robot designed according to a prior software architecture has no way of taking account of how the environment has changed or what parts of a task were performed during an interval of control by a human,

so that errors can occur (and, hence, safety and effectiveness jeopardized) when the human relinquishes control. The present architecture incorporates the control, task-planning, and sensor-based-monitoring features of typical prior autonomous-robot software architectures, plus features for updating information on the environment and planning of tasks during control by a human operator in order to enable the robot to track the actions taken by the

operator and to be ready to resume autonomous operation with minimal error. The present architecture also provides a user interface that presents, to the operator, a variety of information on the internal state of the robot and the status of the task.

This work was done by David Kortenkamp of Metrica, Inc., for Johnson Space Center. Further information is contained in a TSP (see page 1). MSC-23053

Fabrication of Channels for Nanobiotechnological Devices

Nanolithography would not be necessary for establishing channel depths and thicknesses.

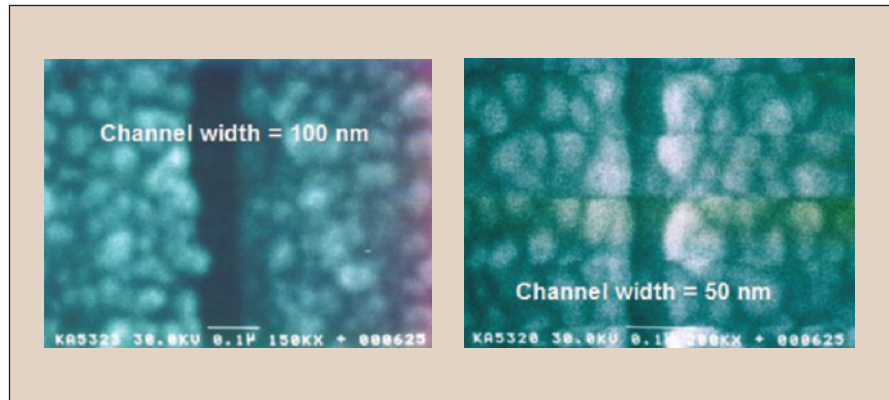
NASA's Jet Propulsion Laboratory, Pasadena, California

A method, now undergoing development, of forming nanochannels in planar substrates is intended to enable the fabrication of advanced fluidic devices that could be integrated with complementary metal oxide semiconductor (CMOS) electronic circuits. Such integral combinations of fluidic and electronic components ("laboratory-on-a-chip" devices) could be used, for example, to detect individual molecules of deoxyribonucleic acid (DNA) and proteins. The width of a channel in such a device would be chosen so that molecules of the species of interest would move along the channel in single file.

In addition to being intended to enable the tailoring of the width of each channel to a uniform value of the order of several nanometers, the developmental method is intended to satisfy the following other requirements:

- A channel must be optically transparent when viewed along a line perpendicular to the plane of the substrate;
- The process of formation of the channels must be compatible with CMOS circuitry and with the processes of fabrication of CMOS circuitry;
- Relative to processes that have been used to fabricate devices containing microchannels, this process must be simple.

In this method, the fabrication of channels includes the use of such CMOS-compatible processes as chemical-mechanical polishing and oxide deposition. The layout of the channels in the substrate plane is determined by a single photolithographic process, but it is not a nanoscale lithographic process, and this process is



These **Scanning Electron Micrographs** show channels of two different widths that were fabricated by the present method. In a finished device, the channels would be covered with an SiO₂ membrane, which would be sufficiently transparent to enable analysis of specimens in the channels by use of a fluorescence microscope.

not relied upon to define the thickness and width of the channels. Stating it from a slightly different perspective, unlike in the prior fabrication of electronic and fluidic devices involving the use of lithography to define microscale features, this process does not include the use of lithography to define nanoscale features. It is this aspect of the method that enables simplification of the process and, hence, a decrease in cost.

A typical fabrication process according to this method includes, among other things, thermal oxidation to form a layer of SiO₂ on a silicon substrate, followed by deposition of a layer of Si₃N₄, followed by deposition of a first layer of polycrystalline silicon (poly-Si). The depth of the channel(s) is determined by the thickness of the first poly-Si layer. The width of the channels (see figure) is determined

by the thickness of the SiO₂ layer, which thickness is readily controllable and can be made extremely uniform.

This work was done by Choonsup Lee and Eui-Hyeok Yang of Caltech for NASA's Jet Propulsion Laboratory. Further information is contained in a TSP (see page 1).

In accordance with Public Law 96-517, the contractor has elected to retain title to this invention. Inquiries concerning rights for its commercial use should be addressed to:

*Innovative Technology Assets Management
JPL*

*Mail Stop 202-233
4800 Oak Grove Drive
Pasadena, CA 91109-8099
(818) 354-2240*

E-mail: iaoffice@jpl.nasa.gov

Refer to NPO-30678, volume and number of this NASA Tech Briefs issue, and the page number.

Improved Thin, Flexible Heat Pipes

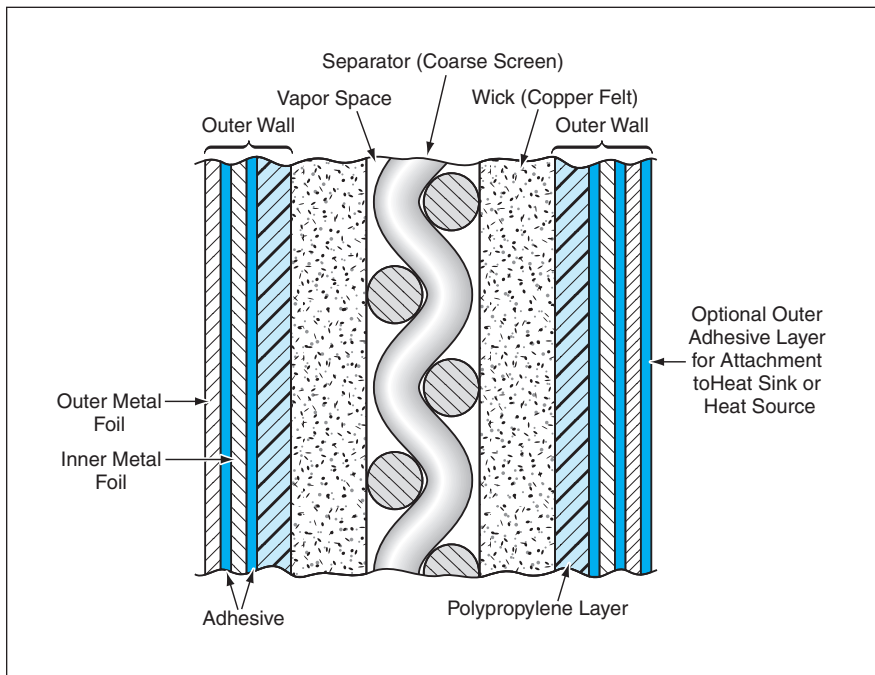
Like common tapes, these heat pipes can be adhesively bonded to curved objects.

Lyndon B. Johnson Space Center, Houston, Texas

Flexible heat pipes of an improved type are fabricated as layers of different materials laminated together into vacuum-tight sheets or tapes. In comparison with prior flexible heat pipes, these flexi-

ble heat pipes are less susceptible to leakage. Other advantages of these flexible heat pipes, relative to prior flexible heat pipes, include high reliability and greater ease and lower cost of fabrication. Be-

cause these heat pipes are very thin, they are highly flexible. When coated on outside surfaces with adhesives, these flexible heat pipes can be applied, like common adhesive tapes, to the surfaces of



A Flexible Heat Pipe can be fabricated as a laminate of polypropylene, metal, and adhesive layers. This enlarged cross section of a typical preferred laminate is not to scale.

heat sinks and objects to be cooled, even if those surfaces are curved.

A preferred design calls for five major layers (see figure) laminated to a total thickness of 0.12 in. (3 mm). The middle layer is a coarse metal (e.g., copper) or polypropylene screen that acts as a separator to maintain the heat-pipe vapor space by separating two other major layers, which are copper felt wicks. The remaining two major layers,

which are sealed together around their edges, are outer walls that constitute the heat-pipe envelope around the wicks and separator. Each outer wall comprises a strengthening sublayer of polypropylene, two sublayers of metal foil, and sublayers adhesive between the polypropylene and metal layers.

The wick layers can be pressed into the polypropylene wall layers (optionally with partial melting of the polypropy-

lene layers) to increase the thermal conductance between the walls and wicks. The two outer walls are joined at their edges by placing their polypropylene layers in contact and then heating them and pressing them together.

The two metal foils in each outer wall serve as barriers against leakage. Because foils occasionally contain random pinholes, one foil layer per wall would not afford sufficient protection against leaks. However, when an outer wall contains two foil layers, it would be necessary for two pinholes to be aligned with each other (a highly improbable occurrence) to make a pinhole leak. Hence, the use of two foil layers per outer wall reduces the probability of pinhole leaks to a small value.

This work was done by John H. Rosenfeld, Nelson J. Gernert, David B. Sarraf, Peter J. Wollen, Frank C. Surina, and John E. Fale of Thermacore, Inc., for Johnson Space Center. Further information is contained in a TSP (see page 1).

In accordance with Public Law 96-517, the contractor has elected to retain title to this invention. Inquiries concerning rights for its commercial use should be addressed to:

Thermacore International, Inc.

780 Eden Rd.

Lancaster, PA 17601

(717) 569-6551

E-mail: info@thermacore.com

Refer to MSC-23400, volume and number of this NASA Tech Briefs issue, and the page number.

Miniature Radioisotope Thermoelectric Power Cubes

These devices could supply power at extremely low temperatures for years.

NASA's Jet Propulsion Laboratory, Pasadena, California

Cube-shaped thermoelectric devices energized by a particles from radioactive decay of ^{244}Cm have been proposed as long-lived sources of power. These power cubes are intended especially for incorporation into electronic circuits that must operate in dark, extremely cold locations (e.g., polar locations or deep underwater on Earth, or in deep interplanetary space). Unlike conventional radioisotope thermoelectric generators used heretofore as central power sources in some spacecraft, the proposed power cubes would be small enough (volumes would range between 0.1 and 0.2 cm^3) to play the roles of batteries that are parts of, and dedicated to, individual electronic-circuit packages. Unlike electrochemical batteries, these power cubes would perform well at low temperatures. They would also last much longer: given that the half-life of ^{244}Cm is 18 years, a power cube could remain adequate as a power source for years, depending on the power demand in its particular application.

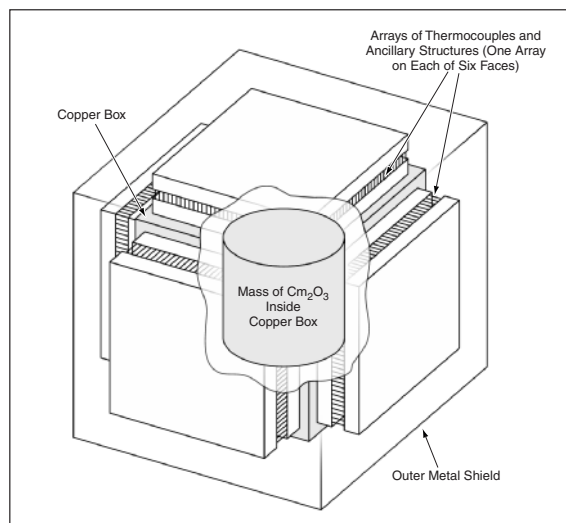
The cubical configuration of a proposed device of this type (see figure) would contribute to thermal efficiency by providing a relatively large area for rejection of heat at low temperature. It would also contribute to thermal-to-electrical energy-conversion efficiency by providing a relatively large heat-transfer area that could be covered with arrays of thermocouples and maximiz-

ing the temperature drop across the thermoelectric elements.

The geometric and thermal heart of a proposed thermoelectric power cube would be a cubic box, made of porous copper, that would enclose a mass of about 0.5 g of ^{244}Cm in oxide form. The wall thickness of the box [≈ 20 mils (≈ 0.5 mm)] would be sufficient to stop the α particles and contain any ancillary radioactivity. The deposition of radioactive-decay energy in the walls of the box would generate heat at the rate of 4.2 W initially, falling to 2.1 W in 18 years. At the initial rate and under typical anticipated operating conditions, this heating would maintain the temperature of the box at about 200 °C.

Thin-film arrays of thermocouples would be mounted on all six faces of the box for efficient conversion of heat into electricity. The portion of the power cube described thus far would be enclosed in a layer of metal that would serve as both a shield and a heat-sinking interface with the environment. The metal shield would also help to contain small amounts of soft γ radiation and neutrons that are emitted from the ^{244}Cm along with the α particles.

According to first estimates, each face



A Power Cube according to the proposal would be designed to exploit synergies among small size, the cubical configuration, and low ambient temperature to obtain relatively high energy-conversion efficiency.

would be covered with about 50 thermocouples that would generate 40 mW of power (a potential of 2 V at a current of 20 mA). Hence, the total electric power produced would be 240 mW, corresponding to an overall thermal-to-electrical energy-conversion efficiency of between 5 and 6 percent.

This work was done by Jagdish U. Patel, Jean-Pierre Fleurial, G. Jeffrey Snyder, and Thierry Caillat of Caltech for NASA's Jet Propulsion Laboratory. Further information is contained in a TSP (see page 1). NPO-30328

Permanent Sequestration of Emitted Gases in the Form of Clathrate Hydrates

Hydrates would be formed under natural conditions.

NASA's Jet Propulsion Laboratory, Pasadena, California

Underground sequestration has been proposed as a novel method of permanent disposal of harmful gases emitted into the atmosphere as a result of human activity. The method was conceived primarily for disposal of carbon dioxide

(CO_2 , greenhouse gas causing global warming), but could also be applied to CO , H_2S , NO_x , and chlorofluorocarbons (CFCs, which are super greenhouse gases). The method is based on the fact that clathrate hydrates (e.g., $\text{CO}_2 \cdot 6\text{H}_2\text{O}$)

form naturally from the substances in question (e.g., CO_2) and liquid water in the pores of sub-permafrost rocks at stabilizing pressures and temperatures. The proposed method would be volumetrically efficient: In the case of CO_2 , each

volume of hydrate can contain as much as 184 volumes of gas.

Temperature and pressure conditions that favor the formation of stable clathrate hydrates exist in depleted oil reservoirs that lie under permafrost. For example, $\text{CO}_2\cdot 6\text{H}_2\text{O}$ forms naturally at a temperature of 0°C and pressure of 1.22 MPa. Using this measurement, it has been calculated that the minimum thickness of continuous permafrost needed to stabilize CO_2 clathrate hydrate is only about 100 m, and the base of the permafrost is known to be considerably deeper at certain locations (e.g., about 600 m at Prudhoe Bay in Alaska). In this disposal method, the permafrost layers over the

reservoirs would act as impermeable lids that would prevent dissociation of the clathrates and diffusion of the evolved gases up through pores.

Because the natural pressure and temperature conditions in suitably chosen reservoirs would favor the formation of clathrates, no additional energy would be needed, other than the energy for pumping the gases into the reservoirs. There would also be no need to drill holes into the reservoirs: instead, the holes and other infrastructure already in place (and used previously to extract the oil from the reservoirs) would henceforth be used to inject the gases into the reservoirs.

As an additional benefit, pumping of CO_2 could help to maintain the pressure necessary for extraction of oil from an adjacent reservoir that had not yet been depleted. At present, natural gas is used for this purpose. The use of CO_2 instead of natural gas would make it possible to recover more natural gas as fuel. Moreover, unlike natural gas, CO_2 does not pose an explosion hazard.

*This work was done by N. Duxbury of Caltech and V. Romanovsky of the University of Alaska at Fairbanks for NASA's Jet Propulsion Laboratory. Further information is contained in a TSP (see page 1).
NPO-30256*

Electrochemical, H_2O_2 -Boosted Catalytic Oxidation System

This system offers several advantages over O_2 -boosted systems.

Lyndon B. Johnson Space Center, Houston, Texas

An improved water-sterilizing aqueous-phase catalytic oxidation system (APCOS) is based partly on the electrochemical generation of hydrogen peroxide (H_2O_2). This H_2O_2 -boosted system offers significant improvements over prior dissolved-oxygen water-sterilizing systems in the way in which it increases oxidation capabilities, supplies H_2O_2 when needed, reduces the total organic carbon (TOC) content of treated water to a low level, consumes less energy than prior systems do, reduces the risk of contamination, and costs less to operate. This system was developed as a variant of part of an improved waste-management subsystem of the life-support system of a spacecraft. Going beyond its original intended purpose, it offers the advantage of being able to produce H_2O_2 on demand for surface sterilization and/or decontamination: this is a major advantage inasmuch as the benign byproducts of

this H_2O_2 system, unlike those of systems that utilize other chemical sterilants, place no additional burden of containment control on other spacecraft air- or water-reclamation systems.

This system produces H_2O_2 in an electrochemical/electrodialytic process that consumes only electrical energy and oxygen; that is, unlike some other systems, this system consumes no expensive chemicals. The system includes an H_2O_2 generator, an H_2O_2 -pervaporation membrane, and an APCOS reactor.

Tests have verified that H_2O_2 can be easily transferred and delivered from a stream identical to that in the central compartment of an electrochemical cell to a required process stream. Test results have also shown that at stoichiometric concentrations, H_2O_2 promotes the increased destruction of urea and of NH_3 (the chief byproduct of urea) in wastewater. Heretofore, NH_3 has been consid-

ered one of the more intractable contaminants for oxidation purposes. Data indicate that oxidation occurs at high rates at low temperatures — an important advantage in that the consumption of energy is reduced and safety increased, relative to prior oxygen-boosted systems that must operate at higher temperatures. Moreover, the ability of this system to oxygenate highly contaminated wastewater was proved by the nearly complete oxidation of 500 mg/L of acetic acid (TOC = 200 mg/L). Considered together, these data are a convincing argument for using electrochemically produced H_2O_2 to boost APCOS oxidation rates in highly contaminated wastewater.

*This work was done by James R. Akse, John O. Thompson, and Leonard J. Schussel of Umpqua Research Co. for Johnson Space Center. For further information, contact the Johnson Commercial Technology Office at (281) 483-3809.
MSC-22708*

Electrokinetic *In Situ* Treatment of Metal-Contaminated Soil

This is an alternative to excavation and to techniques dependent on hydraulic conductivity.

John F. Kennedy Space Center, Florida

An electrokinetic technique has been developed as a means of *in situ* remediation of soils, sludges, and sediments that are contaminated with heavy metals. Examples of common metal contaminants that can be removed by this technique include cad-

mium, chromium, zinc, lead, mercury, and radionuclides. Some organic contaminants can also be removed by this technique.

In the electrokinetic technique, a low-intensity direct current is applied between electrodes that have been im-

planted in the ground on each side of a contaminated soil mass. The electric current causes electro-osmosis and migration of ions, thereby moving aqueous-phase subsurface contaminants from one electrode to the other. The half reaction

at the anode yields H^+ , thereby generating an acid front that travels from the anode toward the cathode. As this acid front passes through a given location, the local increase in acidity increases the solubility of cations that were previously adsorbed on soil particles. Ions are transported towards one electrode or the other — which one depending on their respective electric charges.

Upon arrival at the electrodes, the ionic contaminants can be allowed to become deposited on the electrodes or can be extracted to a recovery system. Surfactants and other reagents can be introduced at

the electrodes to enhance rates of removal of contaminants. Placements of electrodes and concentrations and rates of pumping of reagents can be adjusted to maximize efficiency.

The basic concept of electrokinetic treatment of soil is not new. What is new here are some of the details of application and the utilization of this technique as an alternative to other techniques (e.g., flushing or bioremediation) that are not suitable for treating soils of low hydraulic conductivity. Another novel aspect is the use of this technique as a less expensive alternative to excavation: The

cost advantage over excavation is especially large in settings in which contaminated soil lies near and/or under industrial buildings and therefore excavation would be made even more expensive by the need to prevent damage to numerous underground pipes and cables.

This work was done by Jacqueline Quinn of Kennedy Space Center and Christian A. Clausen III, Cherie Geiger, and Debra Reinhart of the University of Central Florida. Further information is contained in a TSP (see page 1).

KSC-12265

Pumping Liquid Oxygen by Use of Pulsed Magnetic Fields

No moving parts are in contact with the oxygen.

John F. Kennedy Space Center, Florida

An effort is underway to develop a method of pumping small amounts of liquid oxygen by use of pulsed magnetic fields. This development is motivated by a desire to reduce corrosion and hazards of explosion and combustion by eliminating all moving pump parts in contact with the pumped oxygen.

The method exploits the known paramagnetism of liquid oxygen. Since they both behave similarly, the existing theory of ferrofluids (liquids with colloidally suspended magnetic particles) is directly applicable to paramagnetic liquid oxygen. In general, the force density of the paramagnetic interaction is proportional to the magnetic susceptibility multiplied by the gradient of the square of the magnitude of the magnetic field. The local force is in the direction of intensifying magnetic field. In the case of liquid oxygen, the magnetic susceptibility is large enough that a strong magnetic-field gradient can lift the liquid in normal Earth gravitation.

Simple pumps were built to demonstrate the feasibility of the method. Each pump included a 1/4-in. (≈ 6.4 -mm) poly(tetrafluoroethylene) tube, wrapped with several hundred turns of wire. The tube was partially immersed in liquid nitrogen (atmospheric-pressure boiling temperature 77 K), positioned so that the coil was just above the liquid-nitrogen surface. Gaseous oxygen (atmospheric-pressure condensation temperature 90 K) was bled into the tube, wherein it condensed to form liquid oxygen. The coil was connected to and

energized by a pulse circuit as described below. The cooling of the coil by virtue of its proximity to the liquid nitrogen reduces the electrical resistance of the wire significantly, thereby increasing the magnetic field that could be generated by applying a given potential to the coil.

The solenoid coil was subjected to a current pulse through a high-power insulated gate bipolar transistor (IGBT). A typical coil configuration consisted of 1,900 turns of 18-gauge wire, resulting in a solenoid length of 8.3 cm with an approximate resistance of 1/2 ohm at 77 K. Thirty-ampere current pulses of several tenths of a second to 1-s durations, activated the solenoid, while the level of the liquid oxygen (LOX) column was measured. A typical magnetic field of about 0.9 T, accelerated the 36-cm LOX column upward, several centimeters, to just past the top of the solenoid. The dynamics of the LOX column are especially sensitive to starting position near the ends of the solenoid because of the large gradients in the magnetic field. Variations in starting distance of as little as 1 mm can result in 2 or more centimeter variations in maximum displacement of the column.

Part of this work involved the development of a numerical model describing the solenoid electrical circuit and magnetic field characteristics, as well as the LOX dynamics. This model has been shown to agree reasonably well with the experimental data, and like all useful models, it provides a means of carrying

out additional experiments by varying many of the system parameters on a computer. The solenoid drive circuit portion of the model simulates a wide pulse, moderate current using an IGBT (as described above), as well as a short pulse, high current using a charged capacitor. Multiple solenoids with synchronized delayed current pulses were also simulated, suggesting that multiple stage solenoid coils could theoretically propel LOX to any desired distance.

In Earth's gravity, the maximum distance a LOX column can be propelled using a single solenoid, is probably limited to a few inches, dependent upon the size of the column, the specifics of the solenoid, and the available current and voltage. However, in reduced gravitational environments, such as on Mars or in Space, there may be a need to transport small amounts of liquid oxygen and in these lower gravitational fields, significant transport should be possible. An active area of ongoing research is finding a way to produce LOX from the Martian atmosphere. From a reliability standpoint, it may be advantageous to use a pumping system, which requires no moving parts, rather than a mechanical pump that would be more prone to failure.

This work was done by Robert Youngquist, John Lane, Christopher Immer, and James Simpson of Dynacs, Inc., for Kennedy Space Center. For further information, please call the SERTTC Industry Liaison at the Kennedy Space Center Technology Transfer Office, (321) 867-8130.

KSC-12284

Magnetocaloric Pumping of Liquid Oxygen

Neither moving parts nor pulsing of the magnetic field are needed.

John F. Kennedy Space Center, Florida

As noted in the previous article, the field-induced force density on a magnetic fluid is proportional to the magnetic susceptibility times the gradient of the magnetic field squared. The direction of the force is towards increasing magnetic field (positive gradient). Applying a magnetic field to a magnetic fluid will result in a force from all directions towards the location of peak field. Since the magnetic field is conservative and there are no magnetic monopoles, the net field-induced force on any fluid of constant susceptibility will be zero. The only manner to obtain a nonzero net field-induced force is to vary the susceptibility of the fluid. At the gas/liquid interface of liquid

oxygen, the susceptibility varies drastically, and the exploitation of the resultant large net forces has been detailed in the previous article, "Pumping Liquid Oxygen With Pulsed Magnetic Fields" (KSC-12284).

An alternative method of varying the magnetic susceptibility is to vary the temperature of the fluid. The magnetic susceptibility of paramagnetic liquid oxygen obeys the Curie-Weiss law: it is inversely proportional to temperature. By applying a temperature gradient in the presence of a symmetric magnetic field, a nonzero net force results. Much of the theory of the so-called "Magnetocaloric Effect" has previously been developed for and applied to ferromagnetic fluids,

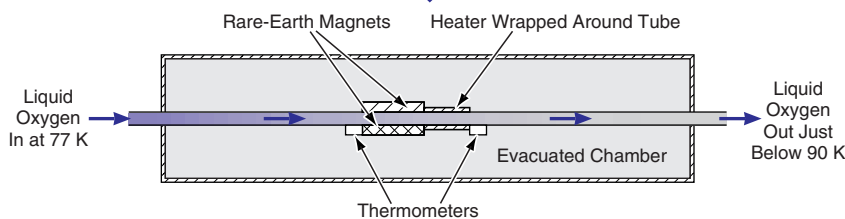
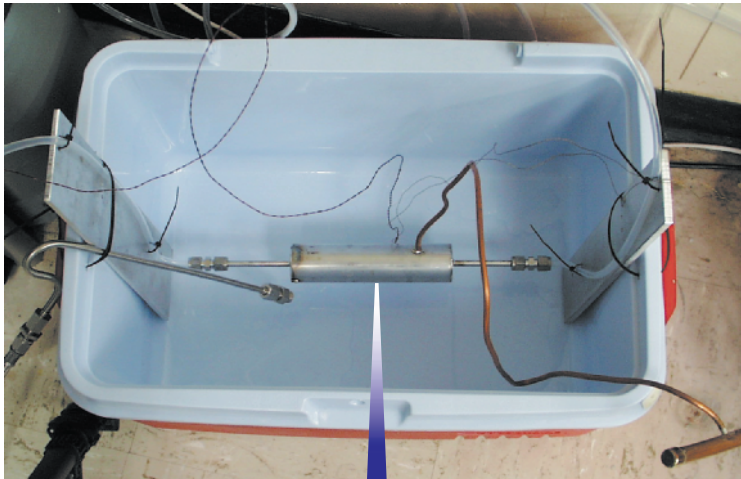
or ferrofluids, but is readily applied to paramagnetic liquid oxygen.

The figure shows an example prototype single-stage magnetocaloric liquid-oxygen pump that has been extensively tested at Kennedy Space Center. Rare-earth permanent magnets supply a peak magnetic field of roughly 0.5 Tesla to a short length of 1/4-in. (6.4-mm) stainless-steel tubing. A heater is placed on one side of the magnets. The assembly is insulated with a vacuum jacket and placed in a bath of liquid nitrogen. The liquid oxygen enters on the left side of the magnetic field at 77 K and is warmed by the heater to just under 90 K on the right-hand side. This 13 K temperature gradient is enough to generate roughly a centimeter of pumping head.

Clearly, many improvements could be made to increase performance. Multiple stages could be juxtapositioned to increase the pumping head. Stronger magnetic field gradients (such as those produced by persistent current mode superconducting magnets) would greatly enhance the force on the fluid. Liquid oxygen at 90 K could be cooled using liquid nitrogen (instead of being warmed by a heater) or cooled by some other means to near its melting point, 54 K, to establish a larger temperature gradient.

Magnetocaloric pumping of liquid oxygen is a way to convert heat directly to motion of the fluid. Being a simple heat engine, it could, in principle, be made to approach the Carnot efficiency. It would also not require any moving parts, would not require contact with the fluid, and would not need access to the edge of the fluid. It would operate in a manner similar to a peristaltic pump.

This work was done by Christopher Immer, Max Kandula, and John Lane of Dynacs, Inc., and Robert Youngquist of Kennedy Space Center. For further information, please call the SERTTC Industry Liaison at the Kennedy Space Center Technology Commercialization Office, (321) 867-8130. KSC-12260



A **Prototype Magnetocaloric Pump** for liquid oxygen has been demonstrated to produce a significant pressure rise.



Tailoring Ion-Thruster Grid Apertures for Greater Efficiency

A report proposes tailoring the diameters of the apertures in the accelerator grid of an ion thruster to reduce the open grid area through which un-ionized propellant gas can escape. The result would be a reduction in the loss of propellant gas and a corresponding increase in propellant efficiency. In a typical ion thruster, the plasma density decreases with radial distance from the centerline, and as a consequence, the diameters of ion beamlets decrease with increasing radial distance. According to the proposal, the apertures, through which the ion beamlets must pass, would be sized to match the diameters (with margin) of the beamlets. The decrease of the aperture diameters with radial distance would result in a significant reduction in the open grid area: In an example based on representative design parameters, the reduction could be as much as 30 percent. In this example, the

transparency to un-ionized propellant would decrease from 0.24 to 0.17 and, as a result, the propellant efficiency would increase from 0.91 to 0.96.

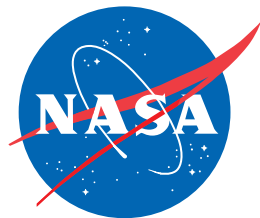
This work was done by John Brophy of Caltech for NASA's Jet Propulsion Laboratory. Further information is contained in a TSP (see page 1). NPO-30625

Lidar for Guidance of a Spacecraft or Exploratory Robot

A report describes the Laser Mapper (LAMP) — a lightweight, compact, low-power lidar system under development for guidance of a spacecraft or exploratory robotic vehicle (rover) at Mars or another planet. The LAMP is intended especially for use during rendezvous of two spacecraft in orbit, for mapping terrain during descent and landing of a spacecraft, for capturing a sample that has been launched into orbit, or navigation and avoidance of obstacles by a rover traversing terrain. The

LAMP includes a laser that emits high-power, short light pulses. The laser beam is aimed in azimuth and elevation by use of a mirror on a two-axis gimbal, which scans the beam across a field of regard. Light reflected by a target is collected by a telescope, and the distance to the target is determined by measuring the round-trip travel time for reflected light pulses. The distance information is combined with directional information to construct a three-dimensional map of targets in the field of regard.

This work was done by Carl Christian Liebe, Robert Bunker, Sohrab Mobasser, Curtis Padgett, Jacob Chapsky, Gary Spiers, Randall Bartman, Michael Newell, Alexander Abramovici, Hemad Hemmati, Alejandro San Martin, Chengchih Chu, William Roberts, Malcolm Wright, James W. Dillon, Daniel S. Clouse, David M. Tratt, Zachary G. Warfield, Robert Calvet, and Robert W. Hausmann of Caltech for NASA's Jet Propulsion Laboratory. Further information is contained in a TSP (see page 1). NPO-30887



National Aeronautics and
Space Administration